



AirCargoChallenge 2022

Technical Report

Team #19

XTRA2 UPV

Xtra2



UNIVERSITAT
POLITÈCNICA
DE VALÈNCIA

Contents

1	Introduction	3
1.1	Air Cargo Challenge	3
1.2	UPV, EUROAVIA València and Xtra2 UPV	3
1.3	Purpose	3
2	Management of the Project	3
2.1	Installations, Equipment and Machinery	3
2.2	Human Resources	4
2.3	Planning and Schedule	4
2.4	Sponsors and Collaborators	5
2.5	Budget	6
3	Conceptual design	7
3.1	Mission Analysis	7
3.2	First Iteration	7
4	Propulsive System	8
4.1	Considerations	8
4.2	Thrust Model	8
5	Aerodynamic Design	9
5.1	Airfoil Analysis	9
5.2	Wing Geometry	11
5.3	Aerodynamic Optimization	12
5.4	Stability and Control	14
6	RC Electronics	16
6.1	Electronic Circuit	16
6.2	Electronic Components	16
7	Structural Design	17
7.1	Considerations	17
7.2	Fuselage, Landing Gear and Empennage	18
7.3	Cargo Bay	19
7.4	Main Wing	20
7.5	Structural Analysis	20
8	Manufacturing Techniques	21
8.1	Empennage	21
8.2	Main Wing	22
8.3	Cargo Bay and Fuselage	23
8.4	Landing Gear and Motor Mount	24
8.5	Results	24
9	Performance in Flight	25
9.1	Polar Plots	25
9.2	Take-off	26
9.3	Climb	26
9.4	Cruise Flight	27
9.5	Payload Estimation	28

10 Conclusion and Outlook	29
Bibliography	30
Appendixes	31
A Similar Aircraft	31
B Drawings	31

1 Introduction

1.1 Air Cargo Challenge

The Air Cargo Challenge is an aeronautical engineering university competition held biennially. The main objective of the competition is to design and build an unmanned aircraft capable of carrying the maximum payload possible according to the competition rules, which vary with each edition.

1.2 UPV, EUROAVIA València and Xtra2 UPV

The Universitat Politècnica de València (UPV) is a Spanish public institution with more than 50 years of history dedicated to teaching and research. It has 2 500 teachers and 30 000 students in its 13 faculties and 42 departments.

EUROAVIA València's headquarters are located on the València campus. The association develops activities related to aviation and space, such as the Xtra2 UPV project, dedicated to the design and construction of radio-controlled aircraft.

The Xtra2 UPV group was founded in 2019 by five second-year aerospace engineering students to participate in the Air Cargo Challenge. Despite their null experience in aeromodelling, they built the Xtra20 model with which they achieved 26th place in the ACC'19. Beyond the result, the team gained experience and advice from other participants to continue progressing.

During the following courses, the group expanded its workforce and built several prototypes. However, the COVID-19 pandemic brought the project to a standstill and forced the postponement of ACC'21. In response, the team developed a preliminary design of the model that would be presented to the 2022 edition and manufactured it with a view to having a quick-to-build, low-cost demonstrator to refine the final model by testing its performance during flight and providing the team with further manufacturing experience.

1.3 Purpose

This report compiles the considerations of the design and manufacturing of the Xtra23 “Favara” model, an unmanned aircraft designed by students of the Xtra2 UPV team of the Universitat Politècnica de València for the Air Cargo Challenge 2022 competition. The report is structured following a chronological order, so that the workflow from the initial design to the final arrangement is illustrated. With this purpose in mind, the document is comprised of eight sections: project management, initial design, propulsive system, aerodynamics, RC electronics, structural design, manufacturing techniques and flight performance.

2 Management of the Project

2.1 Installations, Equipment and Machinery

One of the UPV's faculties, the Escuela Técnica Superior de Ingeniería del Diseño (ETSID), provides the team with a workspace with DIY tools and makes access to 3D printing equipment, CNC laser and hot wire cutter available. The UPV also owns wind tunnels, milling machines or universal testing machines, but this equipment could not be used due to the pandemic situation.

2.2 Human Resources

The Xtra2 UPV team is composed of 36 aerospace engineering students, several collaborators and a professor in charge, Dr. Dr. Michael Tung. The organization chart of the project is shown in Figure 1.

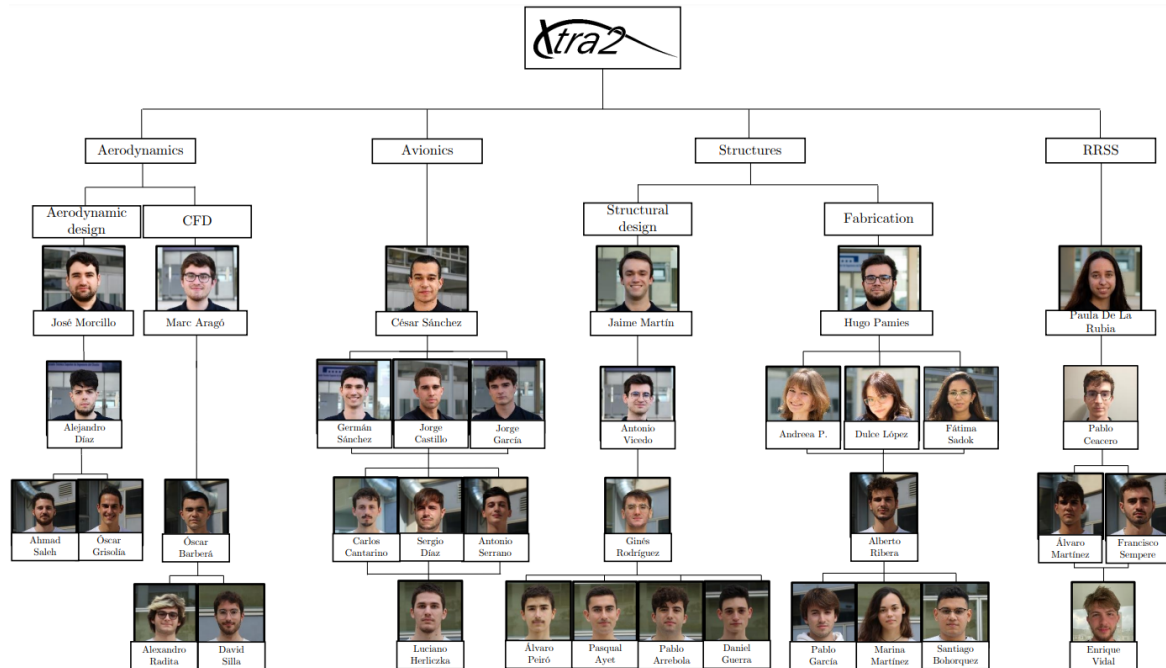


Figure 1: Team organizational structure

2.3 Planning and Schedule

The UPV academic plan is organized in two semesters and four exam periods in total. The planning of this project is based on this organization.

The Xtra23 project schedule has undergone constant changes due to the pandemic. After knowing about the postponement of the event to 2022, it was decided to continue with the established plan during the 2020/2021 academic year in order to build a demonstrator that would allow the final prototype to be improved during the 2021/2022 academic year.

The work plan of both the demonstrator and the final model was based on the UPV academic program, which is divided into two semesters and final exams in January and June in which the project activity is paralyzed. In general terms:

- 2020/2021 course - Demonstrator Prototype
 - First semester (September to January). Preliminary aerodynamic design.
 - Second semester (February to June). Structural design, construction of a low-cost demonstrator model and flight test of the demonstrator.
- 2021/2022 course - Final prototype Xtra23 “Favara”
 - First semester. Improvement of the preliminary design and experimentation with the demonstrator.
 - Second semester. Construction of the final model, report writing and flight tests.

The timetable program for the 2021/2022 course is shown in Figure 2. Notice that “FT” means flight tests. Moreover, in order to meet the schedule programmed for the competition year, the group is organized with the Microsoft Teams platform and meets weekly in a general, technical and/or coordination meeting.

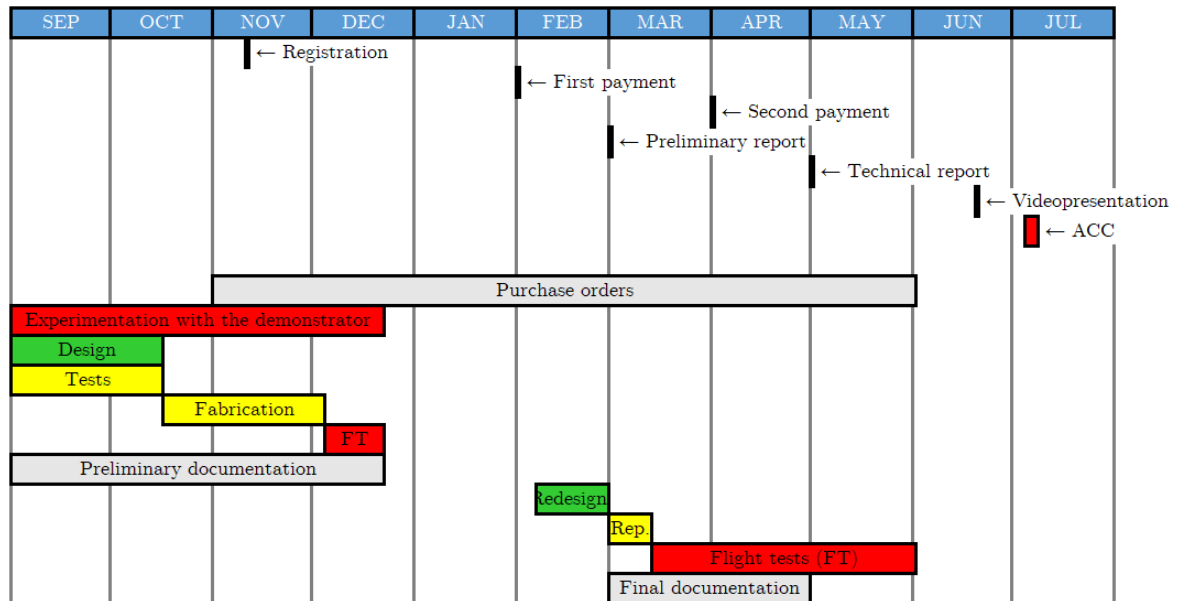


Figure 2: Team organizational structure 2021/2022

2.4 Sponsors and Collaborators

Generación Espontánea (GEUPV): It is an economic program of Universitat Politècnica de València that seeks to promote initiatives of students of this university so that students enhance transversal competences under the philosophy “learning by doing”. During the 2021/2022 academic year, it has contributed 5 495 € to EUROAVIA València to support its activities and projects. Thanks to this support, it has been possible to finance material, tools and part of the registration fees for the competition. In addition to financial support, the UPV also makes MATLAB, Wolfram Mathematica and Office licences available to its students.



Escuela Técnica Superior de Ingeniería del Diseño (ETSID): It is a faculty of the educational institution dedicated to education in engineering areas. It teaches, among others, the Degree in Aerospace Engineering, to which most of the team members belong. It provides the project with workspaces and machinery. It also finances travel and registration to the competition with 3 150 €.



Siemens: It is a conglomerate of German industrial manufacturing companies. It has the Siemens product lifecycle management software section, which is a business unit for Computer-Aided Design, Finite Element Method and Computational Fluid Dynamics software among others. The company offers the team licenses valued at 500 000 €/year for its programs NX, STAR CCM+, Simcenter 3D, AMESim, HEEDS and Fibersim.



AyS-ATS: This group has achieved Smart Expert Partner recognition from Siemens Digital Industries Software with validated exper-



tise in Simcenter 3D. It is in charge of managing the licenses of the team.

Centro de Motores Térmicos (CMT): This is a training and research center of the Universitat Politècnica de València that studies thermo-fluid-dynamic phenomena through experimental and theoretical analysis in its state-of-the-art facilities. It annually sponsors this project by providing facilities and support from its professionals.



Club d'aeromodelisme Ala Partida: Aeromodelling group located in the municipality of Favara, in the south of València. It lends its flying field and facilities to the team. Our final prototype receives its name after the location of this flying field since it is the main one for the team.



Club d'aeromodelisme l'Abella: This club is located in the municipality of La Alcudia, south of Valencia, and is associated with the Federation of Aerial Sports of the Valencian Community. It provides the team with a flying field and advice.



2.5 Budget

The economic value of the project is summarized in Table 1.

ELECTRONICS	COST	CONSUMABLES	COST
Brushless engine	98.00 €	Glue	57.52 €
ESC	43.15 €	Screws (M3, M4)	6.49 €
Batteries	46.99 €	Electronic welding	6.68 €
RX-TX	74.98 €	Adhesive tape	11.97 €
Servomotors	81.00 €	Composite lamination	64.48 €
SUBTOTAL	344.12 €	SUBTOTAL	147.14 €

MATERIAL	COST	ACCESORIES	COST
Balsa wood	23.50 €	Propeller	9.05 €
Carbon fiber	259.07 €	Landing gear	63.40 €
PLA	19.44 €	Oracover	64.10 €
Aluminum	16.08 €	Rods, hinges, extensions	74.60 €
SUBTOTAL	318.09 €	SUBTOTAL	211.15 €

ACC PARTICIPATION	COST
Inscriptions	3 250.00 €
Travel	1 800.00 €
SUBTOTAL	5 050.00 €

TOTAL COST	6 070.50 €
-------------------	-------------------

Table 1: Economic value of the project

3 Conceptual design

3.1 Mission Analysis

The Air Cargo Challenge 2022 promotes the design of very fast and small UAVs yet maximizing the payload as much as possible. The fundamental requirements are [1]:

- Fix wing and defined propulsive system
- The aircraft must be transported in a $1.1 \times 0.4 \times 0.25 \text{ m}^3$ box
- Fast assembly of the aircraft
- The dimensions of the plane are limited to a $1.5 \times 1.5 \times 0.5 \text{ m}^3$ parallelepiped
- Payload consists of blood bags of 100, 200 and 300 g
- Fast loading and unloading times
- Minimum take-off distance of 60 m, plus a bonus if it is under 40 m
- Proper climbing rate
- Maximum travelled distance within a flight time of two minutes

Regarding the limitations, the design is mainly constrained by the regulation in the propulsive system, the dimensions of the aircraft and the take-off distance. From our side, additional limitations are the lack of experience in aeromodelling and the limited access to wind tunnels or milling machines.

Taking into account the requirements, limitations and scoring system, it is established as design philosophy to devise a simple, reliable aircraft that ensures climb rate capacity points as well as the bonus for short take-off. Maximizing payload is targeted as a secondary aim.

3.2 First Iteration

On the basis of the philosophy along with a collection of similar aircrafts, available in Appendix A, the design must meet:

- $x_{to} < 40 \text{ m}$ \rightarrow Short take-off points
- $AR_w > 8$ \rightarrow High aspect ratio to reduce induced drag
- $V_z \geq 2 \text{ m/s}$ \rightarrow Maximize climb rate points
- $t_{min} > 3 : 30 \text{ min}$ \rightarrow Maximum power flight autonomy
- $OEW \leq 2.3 \text{ kg}$ \rightarrow Target operational empty weight

In order to define useful atmospheric variables, a historical data collection of the climate in Munich during daylight hours in July has been used. The reference flight velocity used in the calculations has been set at 11.11 m/s , probably close to the take-off velocity. This is intended to specify the drag coefficient in this phase, which will be assumed constant in the rest of stages, maintaining the design on the safe side. The base proposal reached is seen in Figure 3 and their reference values are displayed in Table 2, where ρ stands for the air density, μ the dynamic viscosity, V the airspeed, c_w the mean aerodynamic chord, S_w the wing surface, b_w the wingspan, c_h the horizontal stabilizer mean chord, and Re_w is the Reynolds number.

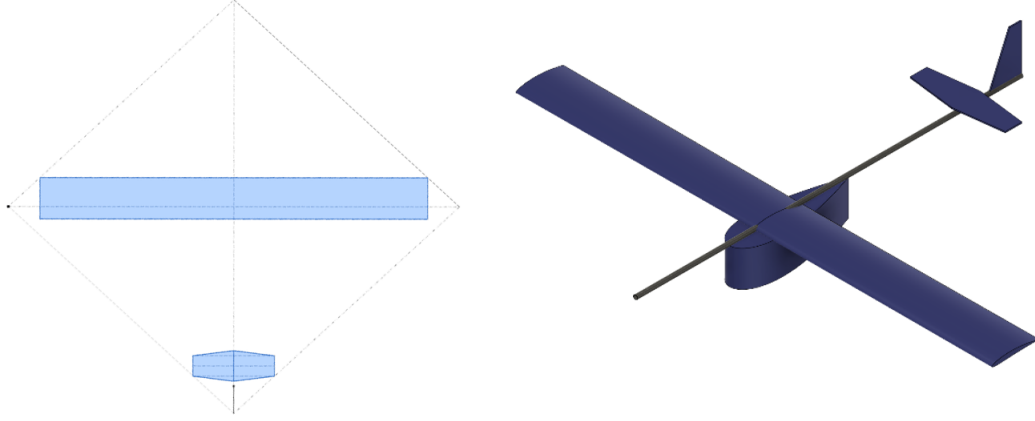


Figure 3: Sketches of the initial proposal for the design

Variable	Interval	Reference
ρ	[1.178, 1.189] kg/m ³	1.189 kg/m ³
μ	[1.822, 1.825] · 10 ⁻⁵ kg/(m · s)	1.825 · 10 ⁻⁵ kg/(m · s)
V	[8.33, 19.44] m/s	11.11 m/s
c_w	[0.18, 0.22] m	0.20 m
S_w	[0.32, 0.44] m ²	0.38 m ²
b_w	[1.80, 2.00] m	1.9 m
c_h	[0.05, 0.15] m	0.10 m
Re_w	[109 000, 253 000]	145 000

Table 2: Reference values established in the conceptual phase

The base design presents a straight wing, traditional landing gear and conventional empennage. This commitment to simplicity seeks the simplification of the manufacturing processes, that will be based on classical structures of balsa wood, given the limitations of the project. The aerodynamic optimization will be focused on wingtip devices, whereas the self-imposed challenge for the team will consist on the use of composites for specific parts of the model.

4 Propulsive System

4.1 Considerations

The motor model fixed by the competition is an AXI GOLD V2 2826/10, while the propeller is to be chosen between two alternatives, both 10x6E. The APC 10x6E propeller has been selected against Aeronaut CAMcarbon Light one due to past problems of the latter in terms of resistance and reliability.

4.2 Thrust Model

Due to the lack of wind tunnel tests, the thrust model has been characterized by means of data provided by APC-Propellers [2], assuming a fixed rotational speed of 9000 rpm, with an empiric correction made with static tests. The thrust can be described by means of Equation 1, where variables use SI units, δ_p stands for the power lever, and T_s for the thrust of the system. In Figure 4 thrust is represented as a function of the airspeed.

$$T_s = \begin{cases} 10.79 \cdot \delta_p & V < 11.38 \\ (10.79 - 0.56 \cdot (V - 11.38)) \cdot \delta_p & V \geq 11.38 \end{cases} \quad (1)$$

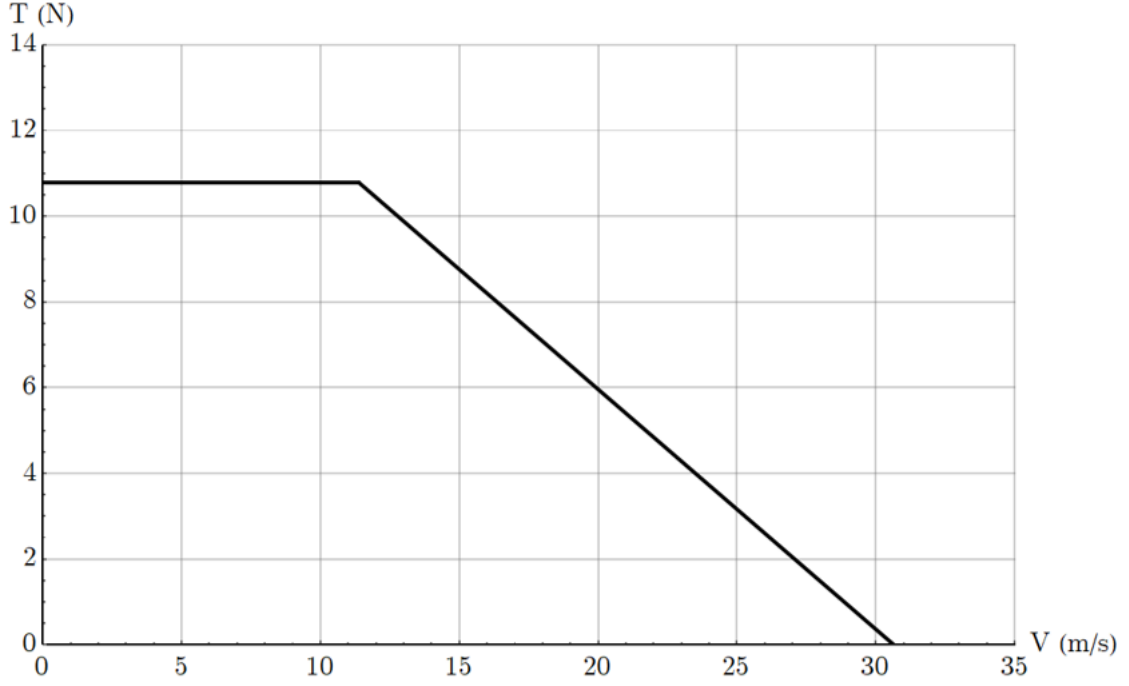


Figure 4: Thrust model

5 Aerodynamic Design

5.1 Airfoil Analysis

Given that the powerplant is fixed by the competition, much of the design weight falls on the aerodynamic section. According to the project philosophy, a good climb rate V_z must be ensured through the reduction of the drag coefficient C_D ; as well as maximizing the maximum take-off weight MTOW through the maximum lift coefficient C_{Lmax} . Additionally, the maximum aerodynamic efficiency EA_{max} , a high stall angle α_{stall} and the lowest moment coefficient C_M are sought.

Taking into account the above criteria, the airfoils represented in the Figure 5 are found in Airfoil Tools [3]. These have been simulated in xflr5 assuming a Re_w equal to 145 000, incompressible regime, standard turbulent transition criterion and iterations for an angle of attack range α from -5° to 20° .

Although airfoils such as AH 79-100 B or SG6043 offer large C_{lmax} values and very high efficiencies, they may not be the most adequate airfoils because of their higher C_{Dmin} or the inability to efficiently balance a wing with such an airfoil. Airfoil A18 is discarded because of its early and abrupt stall. AH 79-100 A and SG6043 are also discarded because of their similarities with other airfoils analyzed.

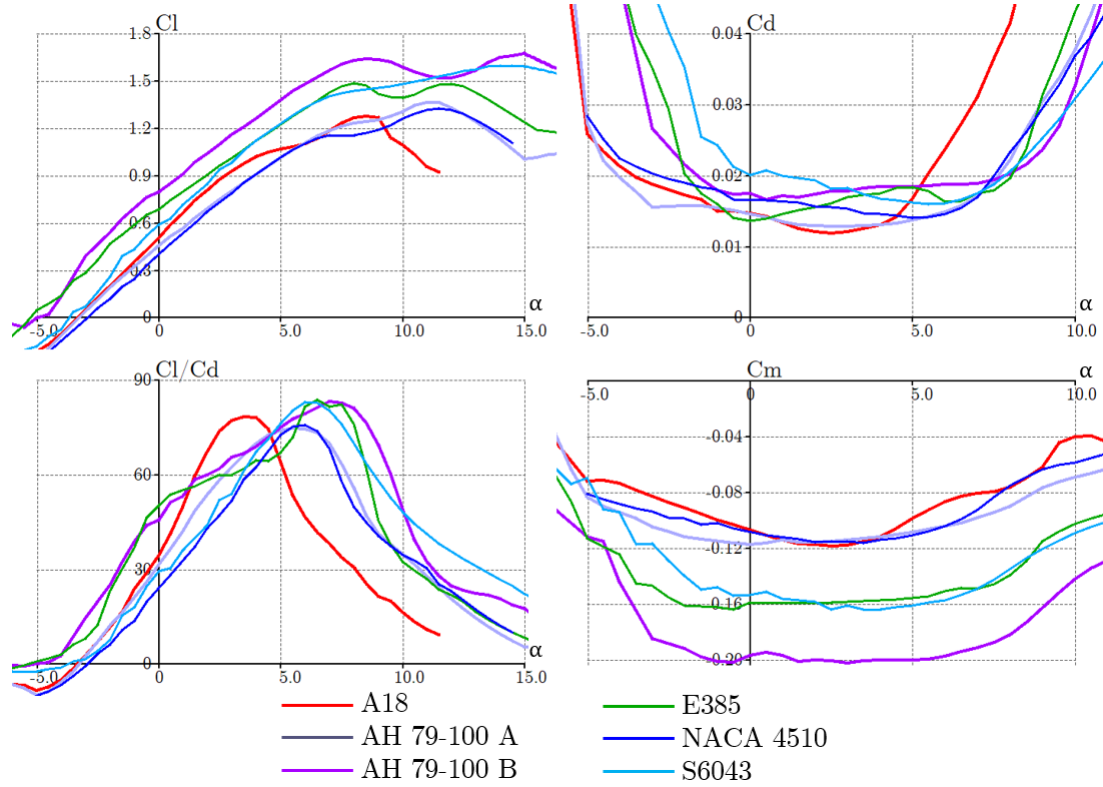


Figure 5: Polar curves of the collected 2D profiles

After two-dimensional analysis, the A 79-100 B, E385 and NACA 4510 airfoils are analyzed in 3D with the nonlinear lifting-line theory (LLT) in xflr5 for geometry and reference parameters. The results shown in Figure 6 indicate:

- The case with the AH 79-100 A presents high C_{Lmax} but also high C_{Dmin}
- The wing with the E385 shows a higher C_D throughout the operating range, in addition to a lower C_{Lmax} and an early stall
- The NACA 4510 offers reduced C_{Lmax} but also lower C_{Dmin} which can maximize climb and horizontal flight speed

Based on the above analysis, the **NACA 4510** profile is selected. This choice is based on the reduced C_{Dmin} of the profile, which should allow to reach high speed in the take-off run and to climb efficiently. In the event that the C_{Lmax} is insufficient, the solution lies in the implementation of high-lift devices.

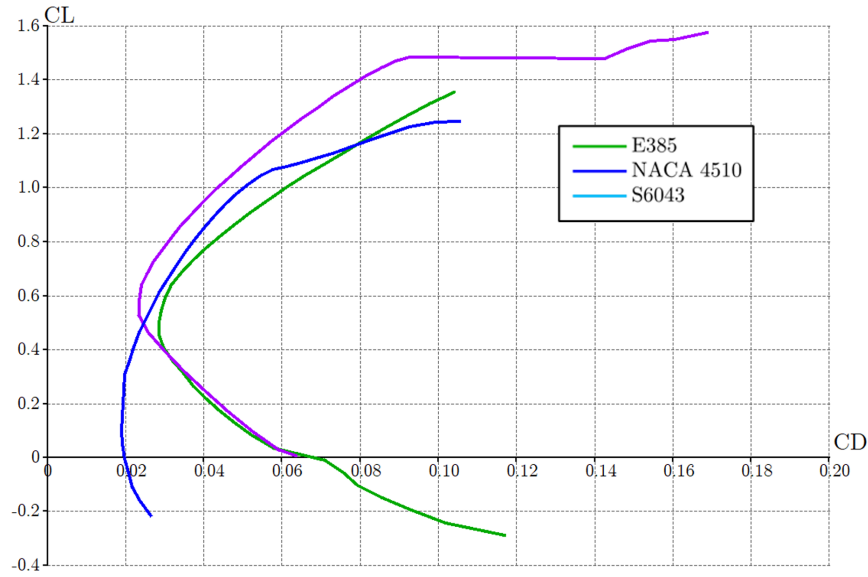


Figure 6: Polar curves of three-dimensional analysis

5.2 Wing Geometry

The preliminary main wing is designed straight, in high wing configuration and without torsion according to the principle of simplicity. No dihedral is included as the center of gravity is expected to lay below the main wing, which already increases lateral stability. To improve performance, wing tip devices are implemented and later optimized in CFD instead of choosing a wing with tapering that would complicate the manufacturing process.

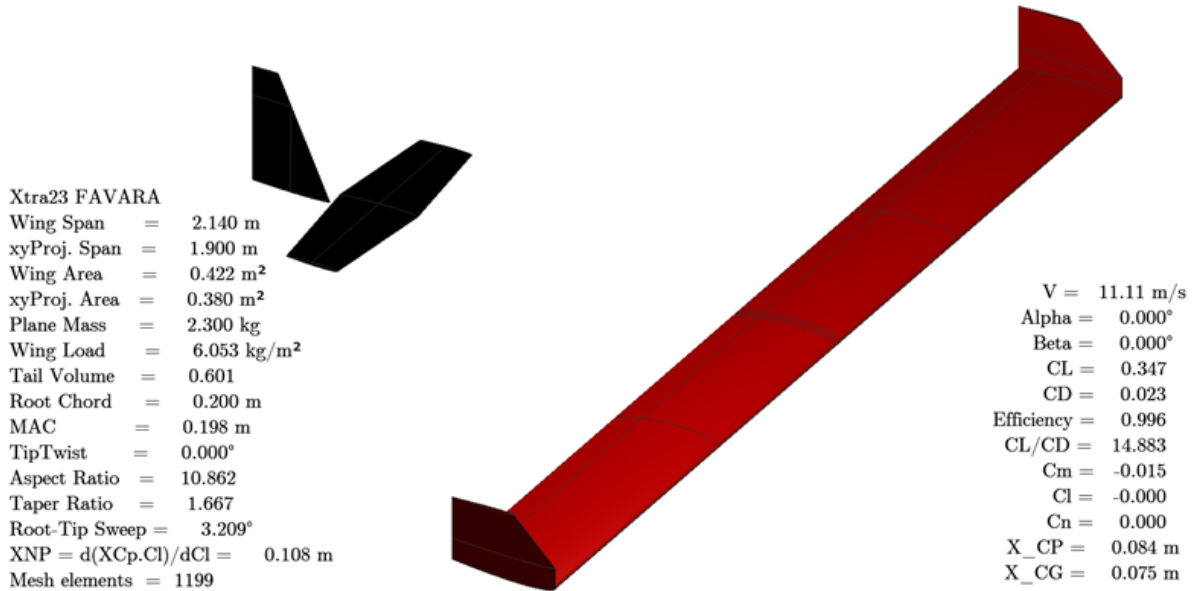


Figure 7: Preliminary design of the wing-empennage assembly on xflr5

The empennage is of conventional type as it is the type that has given the least constructive problems to the team in previous prototypes. This has been designed with a minimalist criterion, with the aim of reducing weight and C_D and increasing the wing area at the expense of static stability. The stabilizers have been simulated with a NACA 0006 profile and their

planforms include some tapering. This idea is based on the increase of surface area in the case of the horizontal stabilizer and on the improvement of the steering rudder control effectiveness in the case of the fin. Additionally, the stabilizer has been raised with respect to the fuselage to increase its efficiency and the fin has been set back to reduce its interference and make better use of the space in the dimensional restriction box.

The proposal that obtained the best performance in relation to aerodynamic efficiency and dynamic stability after an iterative process in xflr5 and experimental tests with a demonstrator is the one shown in Figure 7, which has a c_w of 0.2 m and a b_w of 1.9 m. The polar plots of the final design are shown in section 9 to include the effect of aerodynamic optimization.

5.3 Aerodynamic Optimization

The preliminary aerodynamic design has been achieved using xflr5 Vortex Lattice Method (VLM) simulations, a linear method that interpolates viscous variables from a two-dimensional analysis. This means that it is not possible to optimize those elements whose performance is vital in nonlinear regions such as stall. Therefore, computational fluid dynamics (CFD) is used to design in detail the high-lift devices, winglets and cargo bay. The simulations have been performed with the commercial software Star-CCM+.

The turbulence modeling using CFD software has been developed with two models: $k-\omega$ SST and Spalart-Allmaras. The physical model includes a constant density air model (incompressible model) under normal atmospheric conditions. The simulation velocity was 11.11 m/s. All this has been applied on two types of three-dimensional meshes: Trimmed Cell Mesher and Polyhedral Mesher. Both meshing algorithms have offered a very similar performance in all the cases of study.

Wingtip

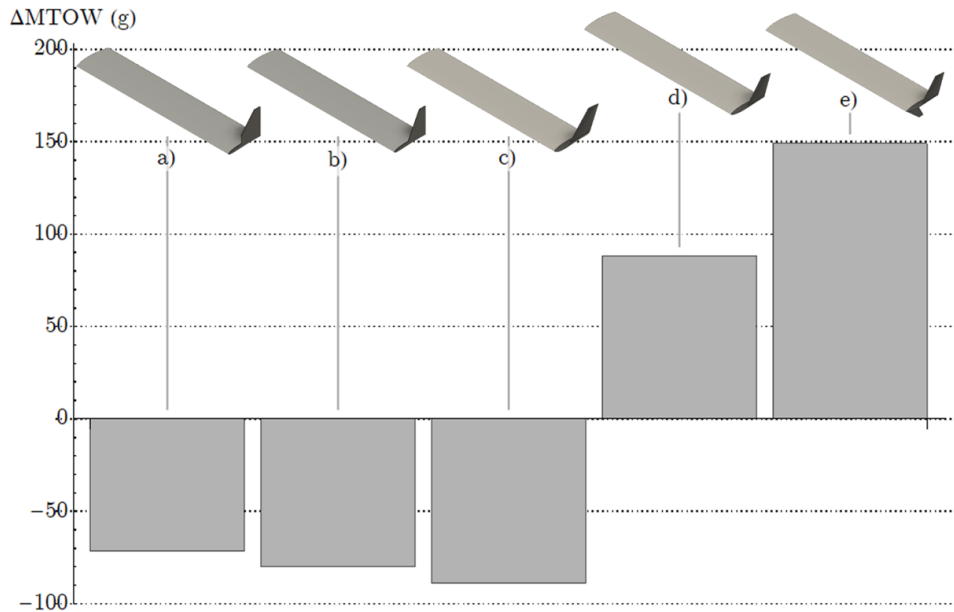


Figure 8: Analysis of the wing tip devices studied

To avoid reducing the wing area, winglets are considered as the most favorable option. In Figure 8 the different designs studied can be seen. The final decision was to build model e),

the Whitcomb Winglet, since the performance offered in terms of MTOW increase is slightly superior to case d), the Blended Winglet. Moreover, it manages to increase the MTOW by about 150 g with respect to the Canted Winglet preliminarily proposed in Figure 7.

High-lift devices

The preliminary aerodynamic design is focused on reducing drag to improve the climb rate but the C_{Lmax} is insufficient. The development of the high-lift surfaces has been carried out by experimental flight tests on the demonstrator and study by CFD software. The problem domain was set to two-dimensional to save computational cost.

In Figure 9 the main designs proposed and tested can be seen. The *Slotted Flap* was the one implemented in the prototype. The sensations given were not satisfactory, causing the aircraft to stall at low angles of attack and significantly worsening maneuverability. Finally, the *Fowler Flap* is the one implemented in the definitive model. It offers a high performance in take-off and low speed landings.

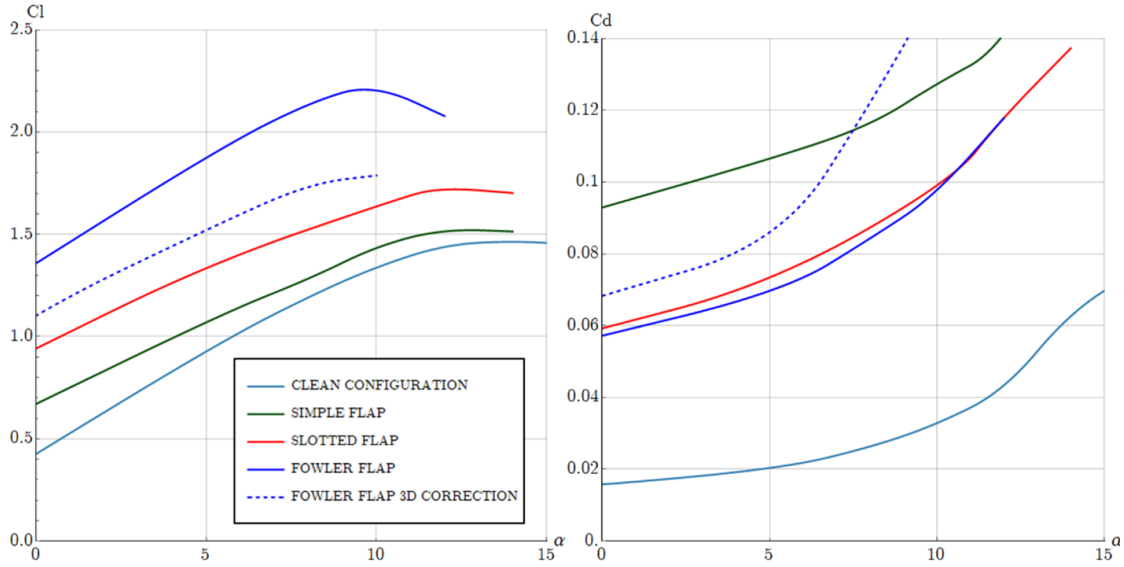


Figure 9: 2D polars of the different flaps under study and 3D correction

Additionally, in Figure 9 a 3D correction on C_L and C_D is represented, based on Equation 2 and Equation 3, where $C_{L\alpha}$, M , $\Lambda_{c/2}$ and C_{LminD} , denote the slope of the lift coefficient with respect to alpha, the Mach number, the swept angle, and the lift coefficient that provides the minimum drag, respectively.

$$C_{L\alpha,3D} = \frac{C_{L\alpha,2D}AR_w}{2 + \sqrt{4 + AR_w^2(1 - M^2 + \tan^2(\Lambda_{c/2}))}} \quad (2)$$

$$C_{D,3D} = C_{Dmin,2D} + \frac{K}{f} (C_{L,3D} - C_{LminD})^2 \quad (3)$$

It has been assumed a value of α corresponding to the null C_L equal in 2D and 3D, an induced constant K adjusted by a 3D analysis of the clean configuration, a reduction factor of the induced constant, f , adjusted by statistical methods and a minimum resistance coefficient equal in 2D and 3D. This last hypothesis is not entirely correct, but will be compensated by the safety factors included in the performance calculation.

Cargo bay

Several geometries have been studied in CFD and experimentally tested for the load bay, as shown in Figure 10. The main problem has been the detachments caused by the cargo bay and how they affect the aerodynamics of the empennage. During flight tests with the manufactured demonstrator with proposal a) from Figure 10, there were some accidents mainly due to the effect of the flow detachment caused by the cargo bay incident on the horizontal stabilizer. The final design has a fuselage geometry that allows to load all the electronics of the aircraft and the loading section is drop-shaped as design c), to minimize the detachments caused by the cargo bay.

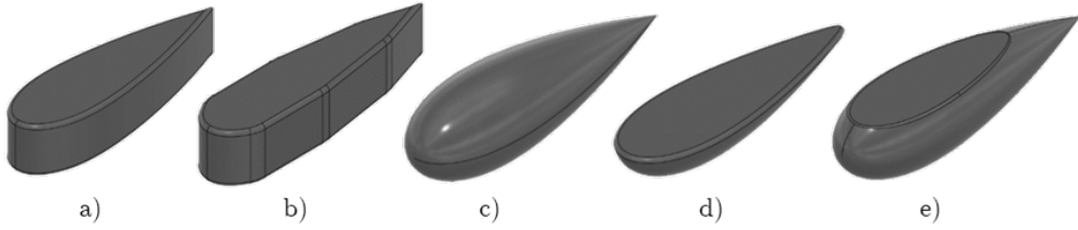


Figure 10: Cargo bays studied

Table 3 collects the most relevant parameters regarding the CFD study of the different cargo bays, where C_{D_0} is the parasitic drag, S_{ref} is the reference surface and the volume of the bay is given in liters.

Case	Volume	S_{ref}	C_{D_0}	Ratio
a)	4.98 l	0.0627 m ²	0.0042	0.0257 N/l
b)	5.14 l	0.0804 m ²	0.0045	0.0267 N/l
c)	7.11 l	0.0478 m ²	0.0055	0.0233 N/l
d)	4.35 l	0.1340 m ²	0.0077	0.0536 N/l
e)	6.5 l	0.1070 m ²	0.0107	0.0498 N/l

Table 3: Results of the parametric analysis of the cargo bay

5.4 Stability and Control

To design the empennage and locate the center of gravity, a moment balance is developed from which the longitudinal, lateral and directional static stability criteria are extracted, indicated respectively from left to right in the Equation 4 [4].

$$CM_\alpha < 0; \quad C\mathcal{L}_\beta < 0; \quad CN_\beta > 0; \quad (4)$$

For a conventional configuration, the longitudinal criterion is satisfied whenever the center of gravity x_{NP} is positioned ahead of the neutral point x_{NP} . Through a simulation with the VLM in xflr5 it is found that the x_{NP} is located at 54% of the mean aerodynamic chord of the main wing. Initially, the x_{CG} was positioned close to x_{NP} with the objective of using the empennage lift to increase the total lift, improve dynamic stability, and reduce the nose length of the aircraft. However, in experimental tests the pilot did not feel comfortable with this configuration. Therefore, although not being the aerodynamically optimal choice, it has been decided to move the center of gravity forward to 37.5% of the chord to increase static stability and the pilot's degree of confidence. This position is constant since the local center of gravity of the payload bay coincides longitudinally with the global center of gravity regardless of the payload.

The degree of longitudinal static stability is quantified through the static margin SM , calculated in Equation 5. This expression also gives the position of the center of gravity and neutral point in mm with respect to the leading edge of the wing.

$$\frac{x_{CG} - x_{NP}}{c_w} < 0 \quad \rightarrow \quad SM = \left| \frac{x_{CG} - x_{NP}}{c_w} \right| = \left| \frac{75 - 108}{200} \right| = 16.5\% \quad (5)$$

On the other hand, the lateral static stability criterion is met by placing the center of gravity below the main wing due to the appearance of a “pendulum effect”. And the directional criterion is verified if the tail fin is able to generate a yawing moment to counteract a sideslip disturbance. Thus, it is obtained and exposed in Equation 6.

$$CM_\alpha = -0.9199; \quad C\mathcal{L}_\beta = -0.0768; \quad CN_\beta = +0.0707; \quad (6)$$

The dynamic stability is adjusted by the length between lifting surfaces, tail area, stabilizer pitch, elevator deflection and center of gravity position. The eigenvalues of the dynamic modes of flight mechanics are computed with the panel method in xflr5 and are plotted in the Figure 11 which, from left to right, shows the roll subsidence mode, short-period, Dutch roll, phugoid and spiral. It shows that at cruising speed without load and with maximum load, all poles are stable and sufficiently damped with the exception of the spiral mode. Nevertheless, this pole is slow enough so that it can be corrected by the pilot during flight. In addition, it should be noted that the airframe contribution has not been simulated and that this is a linear analysis, which introduces some uncertainty to the numerical model.

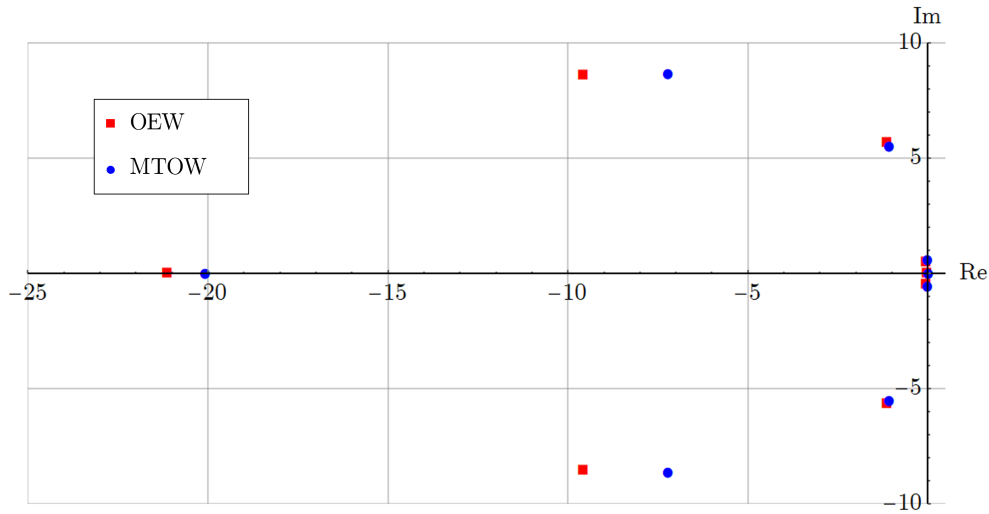


Figure 11: Representation of the root locus of the dynamic stability modes

The control surfaces must allow the aircraft to maneuver adequately to perform its mission. The flight circuit does not present obstacles that require an aggressive control configuration, but can be flown freely in the flight area that allows 180° turns of a maximum radius of approximately 65 meters in the limit case. Even so, it was decided to provide the aircraft with a relatively aggressive flight performance to avoid the maneuverability problems presented by the team’s previous prototypes.

After an iterative process, the primary control surfaces are sized as shown in Table 4, where δ denotes the maximum deflection of the respective surface, the subscript w refers to the main wing, h to the horizontal stabilizer and v to the vertical stabilizer. These were designed according to controllability criteria such as elevator deflection to trim at the desired speed or maximum achievable roll rate after maximum deflection of aileron or aileron combined with rudder. These studies are plotted in Figure 12.

	c_f	b_f	δ_f
AILERON	$[0.75, 1.00] c_w$	$[0.50, 1.00] b_w$	$[-25^\circ, +25^\circ]$
ELEVATOR	$[0.50, 1.00] c_h$	$[0.00, 1.00] b_h$	$[-20^\circ, +10^\circ]$
RUDDER	$[0.69, 1.00] c_v$	$[0.00, 1.00] b_v$	$[-25^\circ, +25^\circ]$

Table 4: Relative dimensions of the control surfaces

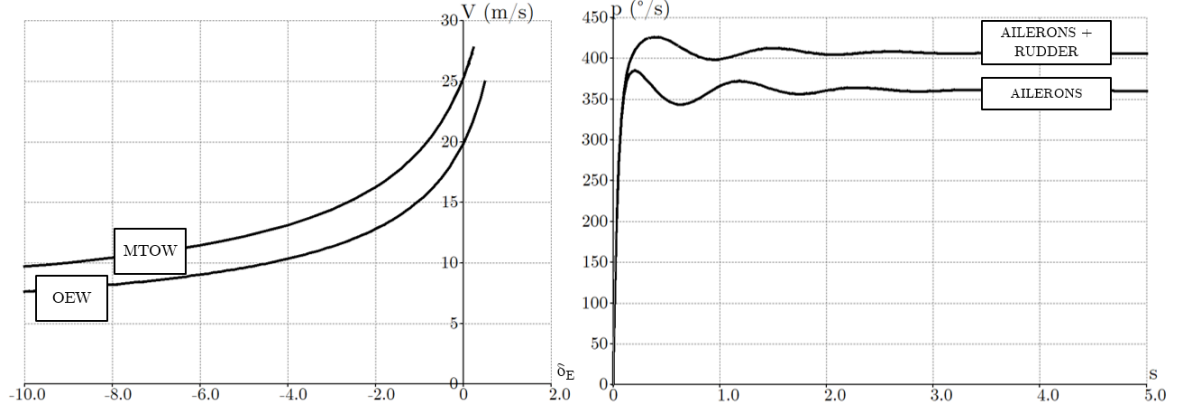


Figure 12: Aircraft maneuverability criteria. On the left, trim speed as a function of elevator deflection; on the right, roll rate evolution

6 RC Electronics

6.1 Electronic Circuit

The electronic circuit is composed by the motor, fixed by the competition, the Electronic Speed Controller (ESC), both main and auxiliary batteries, the receiver, and the servomotors. They are schematically disposed as shown in Figure 13 and described in subsection 6.2.

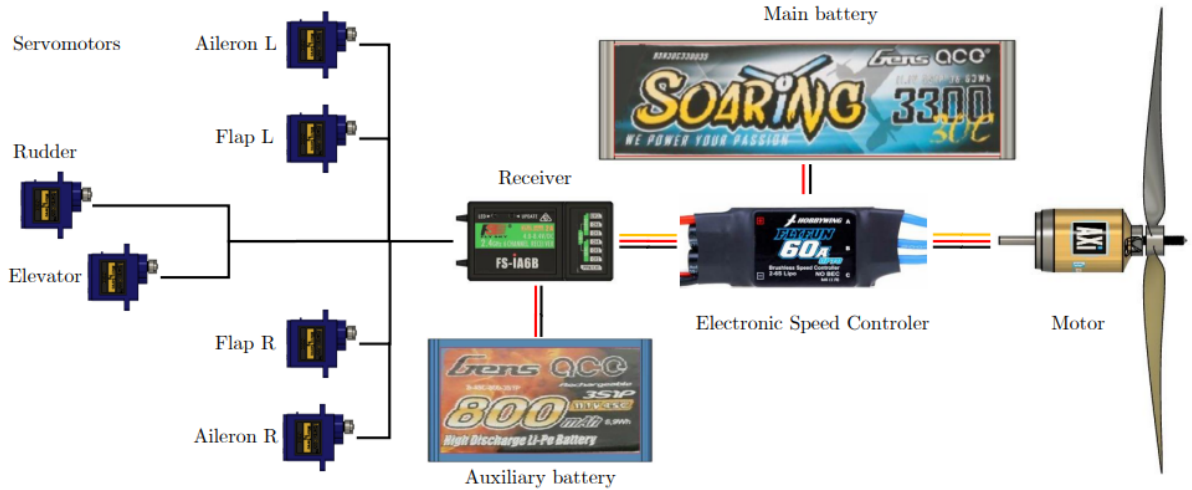


Figure 13: Electronic circuit scheme

6.2 Electronic Components

Electronic Speed Controller: defined by the maximum intensity that it needs to withstand, calculated according to the specifications of the motor. In this case, the maximum

amperage ($I_{max,m}$) that the motor demands is 42 A, so that a commercial 60 A ESC must be selected. Currently, two ESC models are used in the aircraft, “Hobbywing FlyFun 60A V4 OPTO” and “SUPPO ESC 60A”, both capable of withstanding three-cell batteries. The use of the first one is prioritized because of its higher quality and lower weight.

Main battery: the limitations imposed by both the ACC rules and the motor restrict the battery to a 3S one, with a discharge rate of at least 15 C. Taking into account a maximum flight time (t) of 210 s, while introducing a security factor (n), Equation 7 is used to calculate the capacity of the battery at maximum power supply. It has to be noted that landing and missed approaches are not included in t since maximum power is not required for these phases; instead, they are contemplated in n as well as the fact that available capacities of commercial batteries do not match the calculated q_{bp} , so that the next higher capacity available is chosen.

$$q_{bp} = n \cdot t \cdot I_{max,m} = 1.2 \cdot \frac{210}{3600} \cdot 4300 = 3010 \text{ mAh} \quad (7)$$

Among the providers of the Xtra2, and due to the reliability that is intended for the aircraft, the final selection is a 3 300 mAh Gens ACE battery, with a nominal voltage of 12.6 V (3S) and a discharge ratio of 30 C, weighting 252 g. The capacity margin contemplates motor maneuvers as well as the possibility of a missed approach.

Servomotors: moving from the untrustworthy plastic gear motors that had been traditionally used within the team, it has been opted for the use of metallic gear servomotors despite their higher price. The torque that each servo needs to exert, later verified by CFD simulations, has been calculated by means of Equation 8, where c_f is the chord of the moving surface in cm, b_f its length in cm, V stands for the airspeed in mph, δ_f represents the deflection of the given surface and θ_f the operational range of the servo from the neutral point. [5]

$$T_{servo} = 6.12 \cdot 10^{-7} \cdot \frac{V^2 \cdot c_f^2 \cdot b_f \cdot \sin(\delta_f) \cdot \tan(\delta_f)}{\tan(\theta_{servo})} [\text{kg} \cdot \text{cm}] \quad (8)$$

The suitable servomotor model available is the “Towerpro Digital MG92B”, with 3.1 kg cm at 5 V, that fulfils with the specifications of the aircraft.

Receiver: consists on a FlySky FS-iA6B receiver, which has support for as many channels as required by our project.

Auxiliary battery: a 2S LiPo Gens ACE battery of 800 mAh has been chosen to be able to supply power to the attitude control circuit.

7 Structural Design

7.1 Considerations

Structural design has for objective to minimize the empty weight of the aircraft, fulfil the transportation box specifications and to obtain enough structural endurance to overcome the static bending test. Stiffness and lightness of composite materials based on carbon fiber (CF) have been the best to perform in almost every occasion in the last editions of the ACC, given that the optimal designs required longer wingspans and lengths. However, the dimensional restrictions for the ACC’22 make wingspans of more than 2 m long almost impossible to be designed.

It has been concluded that this year the use of composites will not be as determinant, and hence the use of shell-type wings. Being the experience of our team based on the classic rib-spar

structure, we opt for the design of a traditional wing, made basically of balsa wood. At the same time, the development of our team is crucial, and thus we have set the self-challenge of laminating for the first time some parts of our aircraft in composite materials. Additionally, 3D printers will be used with lactic poliacid (PLA) and machined aluminum will serve as some of the joints.

The main materials used in the project and their properties in the weak direction, for the anisotropic materials, and in order to get a sufficient level safety, are shown in Table 5 [6].

	CF	Balsa wood	PLA	Aluminum
Density	157 kg/m ³	150 kg/m ³	1240 kg/m ³	2700 kg/m ³
Young's Modulus	133 GPa	1.14 GPa	1.12 GPa	69 GPa
Bending strength	500 GPa	14.90 GPa	48.00 GPa	260 GPa
Tensile strength	2200 GPa	2.00 GPa	48.00 GPa	310 GPa

Table 5: Summary of the physical and mechanical characteristics of the employed materials

7.2 Fuselage, Landing Gear and Empennage

The fuselage is mainly a pre-manufactured CF tube of 18 mm of external diameter and 1.30 m of length. The objective of this minimalist philosophy is to reduce the weight and drag. Given that the transportation box limits its length to 1.18 m, the team has decided to divide it in two parts, front and rear fuselage, which are fixed to each other by means of a clamp and attached to the cargo bay and the empennage.

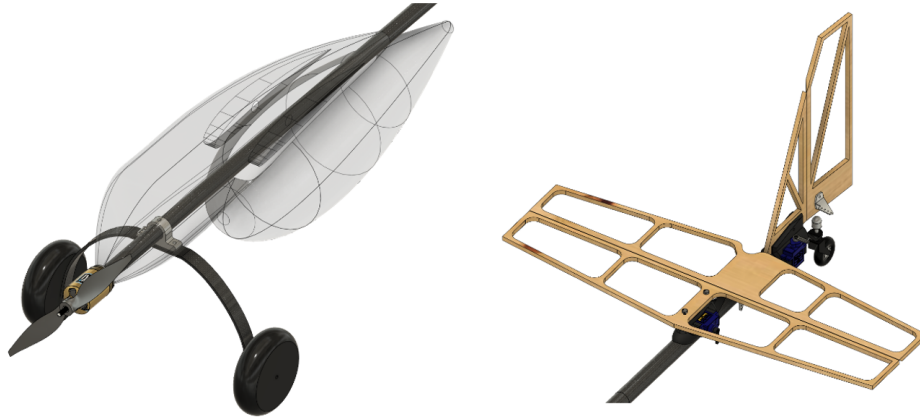


Figure 14: Front and rear fuselage, on which other systems are mounted

In the front part of the fuselage, displayed in Figure 14, the motor is placed through an aluminum joint made by turning. The main landing gear is also joined to the fuselage by means of a mechanized aluminum structure, this one made by milling, which is hidden by the cargo bay. The landing gear is a conventional one, because of its simplicity in assembly, reduced drag and reliability in grass and concrete. Every component of the landing gear is commercial, manufactured in CF for the structure and polyurethane foam for the wheels. The rear wheel, made out of plastic, is placed at the end of the fuselage within the empennage. The structure of the stabilizers is designed for a 5 mm plate of balsa wood to simplify the manufacturing process. Its joints are a critical element as they must be rigid and well adapted. Because of that, they are modelled in a thermoplastic material to be produced by extrusion.

7.3 Cargo Bay

This subsystem must bear and contain the payload bags, limit their movements and maximize accessibility. The most common typologies are the external to the fuselage and the integrated cargo bay. As the fuselage is a cylindrical tube, we have chosen the external bay, as proposed in the conceptual design of Figure 15, to facilitate the manufacturing process and improve accessibility in decrement of the aerodynamic properties. In the preliminary design, a NACA0030 profile was chosen against the water-drop-shaped bay due to a simpler manufacturing, as the aerodynamic design did not make a sufficient difference between them for a null angle of attack. The architecture is based on a shell of carbon fiber and an internal structure of plywood. For the first experimental probes, a reduced-cost cargo bay was built in balsa wood and plywood.

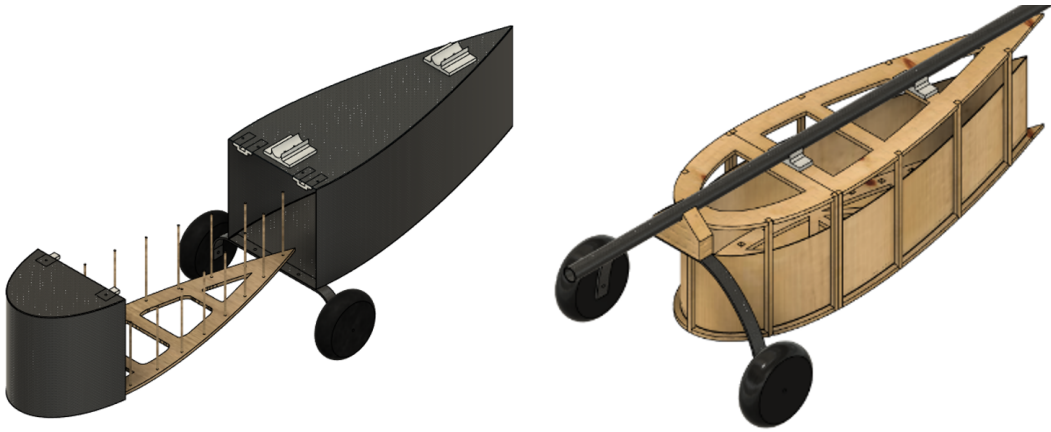


Figure 15: Preliminary cargo bay on the left and experimental on the right

However, during the flight tests the demonstrator suffered an accident because of the incident turbulent wake on the empennage due to the increase in the angle of attack. Consequently, this element was redesigned to have the shape of a water drop and to harbor the electronics. The frontal gate to access it is seen in Figure 16. The definitive design, lighter and more aerodynamic, also includes a better joint to the fuselage and main wing. The gate to introduce the payload is in the rear part of the CF built bay, it counts with a hinge and a latch and it can transport up to 8 bags of 300 g, even if that is more than our MTOW, which means that it can be optimized even more. To avoid the movement of the payload when the bay is not completely full, expanded polystyrene (XPS) walls are introduced.



Figure 16: Definitive cargo bay

7.4 Main Wing

The main wing has been divided in two parts which get together through the flanks of the cargo bay. Its internal structure, visible in Figure 17, is made by:

- Ribs, spars and stringers of balsa wood, 3 to 6 mm width
- Leading edge reinforcement in CF, laminated by ourselves
- Pre-manufactured carbon fiber tube to join both wings and bay

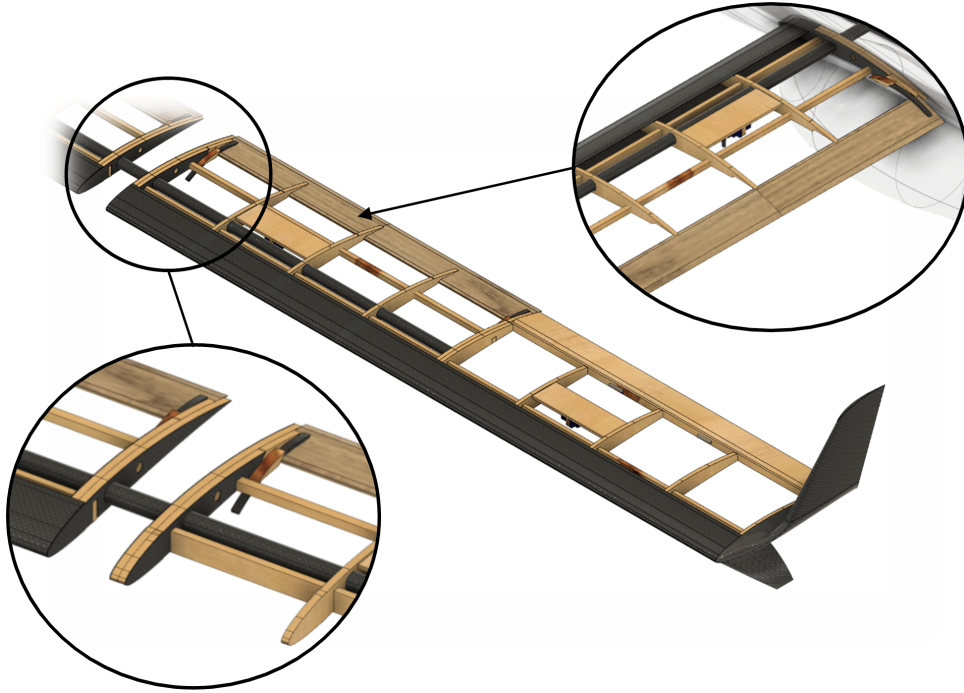


Figure 17: Internal structure of the main wing; detail in the socket and the flap

The rib in the socket is a compound of balsa wood and carbon fiber, and has a nut to avoid wear if fixed to the wood itself. To distribute the structural loads and help the covering of the wing with oracover, a thin layer of balsa wood (1 mm) is placed all over the wing.

Winglets are designed as a composite material shell. To make them more rigid, a balsa wood structure has been built inside of them, as seen in Figure 22. Control surfaces are also solid balsa wood pieces which are joined to the wing by means of nylon hinges, except for the Fowler flap. Its extension mechanism, in contrast to other robust systems seen in previous ACC editions [6], maintains the minimalist philosophy of the whole design, as it is based on a simple slider designed to be a CF sheet through a 3D printed guide. The actuation system of all the control surfaces is a push-pull type and has a metallic rod in contact with a horn made of nylon screwed to the mobile surface and with the servomotor arm. Even though it is recommended that this mechanism is kept inside the structure [7], this has not been possible due to the reduced thickness of the wing.

7.5 Structural Analysis

The most important structural loads in an aircraft are usually the bending loads over the main wing. Cruise phase can be modelled as a cantilever with a distributed load along half of the wing, but the static bending test with the payload is much more critical than the normal

operation of the aircraft, which does not need to overcome such aggressive maneuvers. This case can be modelled assuming:

- The CF joint spar extends to the whole wingspan, bears all the loads and simplifies to beam supported by its tips
- The maximum mass of the system is modelled as a force applied to a point at half of the wingspan
- Mass of the wing is neglected against the total mass
- Only normal stresses are considered by bending moment

Considering the Bernoulli-Euler and Navier equation with the values in Table 5 and the inertial and geometric parameters of a CAD model, we obtain for the MTOW a sufficient Safety Factor (SF) to easily overcome the structural test, in accordance with Equation 9 and Equation 10. Additionally, the force, moment and displacement are shown in Figure 18.

$$\sigma_y = \frac{M_x}{I_x} z \rightarrow \sigma_{y,max} = 58.14 \text{ MPa} \quad (9)$$

$$SF = 8.59 \quad (10)$$

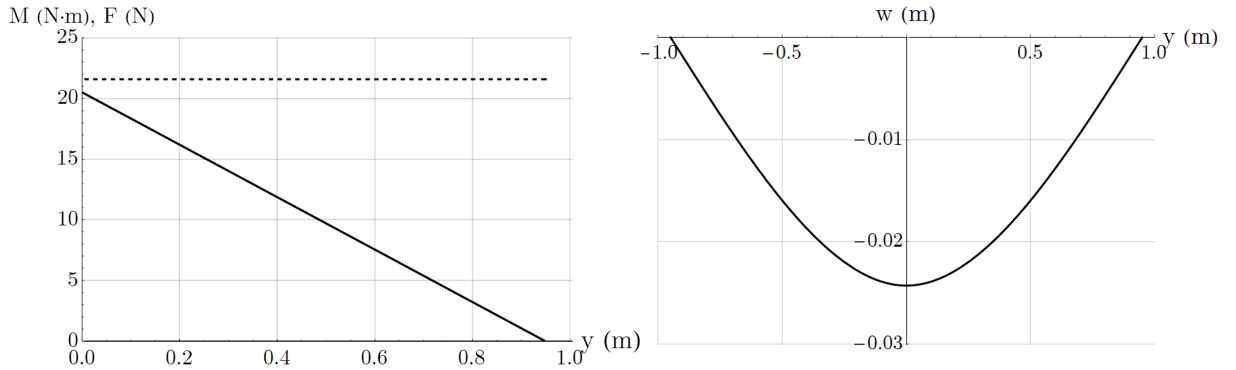


Figure 18: Force, bending moment and displacement from the structural analysis

8 Manufacturing Techniques

8.1 Empennage

The stabilizers are simply a laser-cut flat plate that are connected to their fuselage attachment piece by means of M4 screws. These surfaces, together with the control surfaces, require a sanding process to smooth their edges. Once they are shaped, the structure is covered with thermo-adhesive plastic film.

For the construction of small parts with complex geometry such as the joints of the stabilizers (Figure 19) or the horns of the control surfaces, 3D printing has been used.

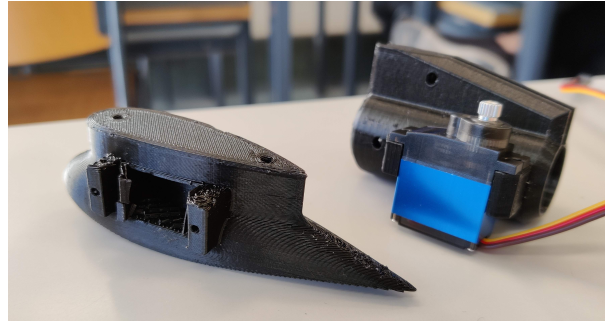


Figure 19: 3D printed joints for the empennage

8.2 Main Wing

The main wing (Figure 20) consists of a prefabricated CF tube, a CF leading edge stiffener of hand laminated CF and laser cutter-formed balsa wood components. All of these are rigidly joined with vinyl glue and the entire structure is attached with M4 bolts to the bay. 3D printing is a method that is also used to manufacture the molds for the leading edge and winglets as seen in Figure 21. Given the small dimensions of the machine, these components are printed in several parts that are then glued with epoxy resin, and finally their surface is made uniform by applying a layer of putty to correct irregularities and another layer of resin for a smooth finish.

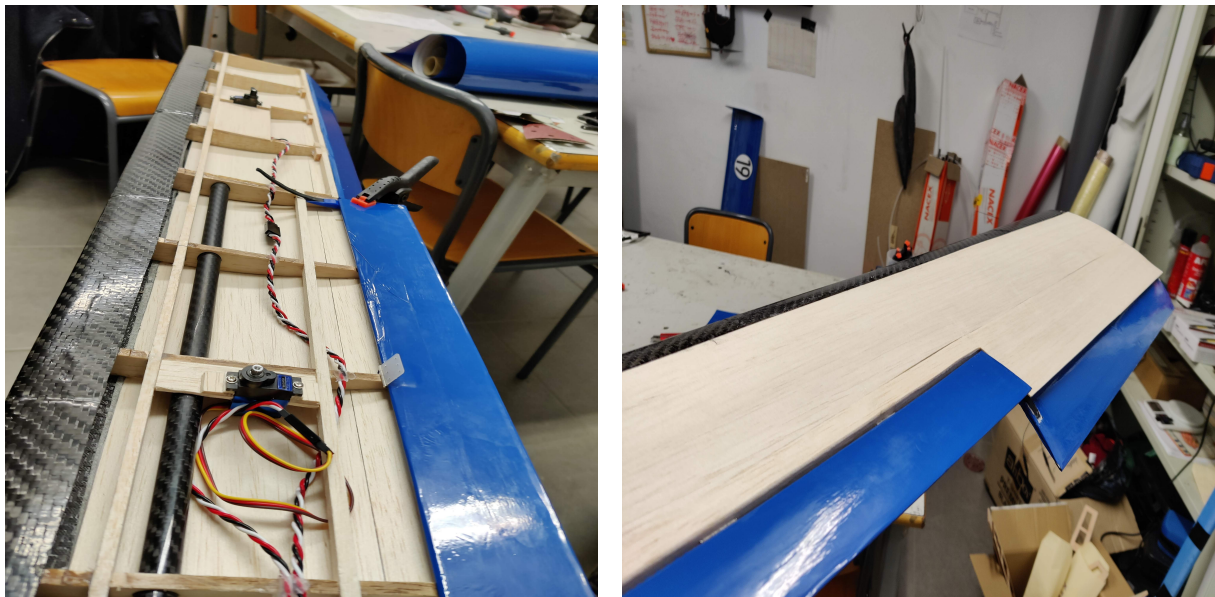


Figure 20: Internal structure of the wing and upper side of the main wing

Formed composite elements require two types of manufacturing processes: without mold, for simple and sandwich-like structures; and in open mold by hand lamination, for complex geometries. The matrix used is vacuum-cured epoxy resin at room temperature and the reinforcement is generally made by two layers of 160 g CF twill. For the winglets, an 80 g unidirectional CF layer and an outer 80 g glass fiber (GF) plain weave layer were experimented with, but the stiffness was not as expected, so the part was reinforced with an internal hand cut balsa structure. This process can be seen in Figure 22.



Figure 21: 3D printed winglet molds



Figure 22: Internal structure of the winglet

8.3 Cargo Bay and Fuselage

The cargo bay is an element that integrates a compartment for the bags carried, a space to incorporate the electronics, a box containing the measuring system, as well as the connection with the main wing and the fuselage. It has a very complex geometry and has therefore been manufactured in CF by vacuum lamination, as seen in Figure 23, in several steps.



Figure 23: Vacuum lamination of the cargo bay

As it is composed of two symmetrical pieces, it is assembled by applying two-component structural adhesive based on epoxy resin along the longitudinal axis. Subsequently, the accesses to the cargo compartment, electronics space and measuring system mount are cut out with a precision disk saw. Using magnets, a hinge and a metal locking mechanism, the access doors to the interior of this structure are installed.

8.4 Landing Gear and Motor Mount

The landing gear consists of a standard YAK 55 1000 part prefabricated in CF, two foam wheels with 4 mm axles, and a connecting part machined in aluminum exclusively for this application. To manufacture it, a CNC milling machine has been used to make the contour. After this, a manual milling machine was used to drill the holes for the screws that anchor the landing gear, and the hole through which the 18 mm tube that acts as a fuselage passes. In a similar way and also in aluminum, the part that fixes the engine to the rest of the aircraft has also been machined. In this case, the method used is manual turning, followed by several drilling operations for the screw holes. In this way, two very robust joints are obtained that limit any type of displacement or rotation.

8.5 Results

After the assembly process it is verified that it is possible to properly balance the Xtra23 “Favara” prototype with an OEW of 2.271 kg assuming that the data measurement system delivered by the organization has a mass of 150 g. The mass and distribution of each element is summarized in the table below.

COMPONENT	m (kg)	x_{cg} (mm)	z_{cg} (mm)
Motor and propeller	0.234	− 290	− 18
Main landing gear	0.092	− 90	− 99
ESC	0.058	− 190	+ 5
Main battery	0.235	− 190	+ 5
Auxiliary battery	0.046	− 190	+ 18
Rx and connectors	0.037	− 120	+ 10
GPS	0.150	− 42	+ 20
Cargo bay	0.346	+ 75	− 55
Fuselage	0.303	+ 360	− 18
Main wing	0.630	+ 84	+ 10
Stabilizer	0.077	+ 865	+ 2
Tail fin and skid	0.063	+ 1039	− 8
OEW	2.271 kg	+ 75 mm	− 11 mm

Table 6: Mass and position of each component with respect to the leading edge

Figure 24 shows the final appearance of the Xtra 23 “Favara” once assembled and ready for its first flight in April 2022. This test demonstrates its performance capabilities and maneuverability characteristics, very consistent with those estimated during the design phase.



Figure 24: Pre-flight image of the completed aircraft

9 Performance in Flight

9.1 Polar Plots

Applying a linear mathematical model and considering the parabolic polar of constant coefficients for the aerodynamic drag, the polar curves plotted in Figure 25 are obtained and employed to study the performance of the aircraft.

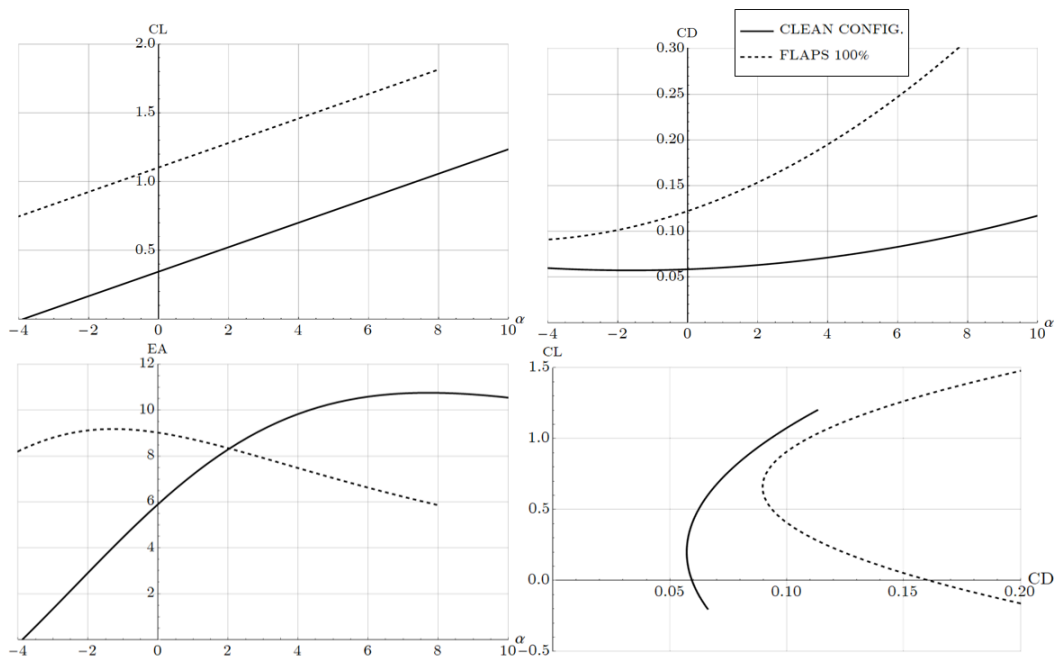


Figure 25: Definitive polar curves for a velocity of 11 m/s

9.2 Take-off

The distance needed to take off depends on the aerodynamic, traction, weight and friction forces, as reflected in Equation 11.

$$x_{to} = \frac{W}{g} \int_0^{V_{to}} \frac{V}{T_s(V) - D(V) - \mu_d(W - L(V))} dV \quad (11)$$

Where it has been considered that:

- The runway is horizontal
- A friction coefficient μ_d for grass of 0.1 [4]
- A safety factor of 20% for the maximum lift coefficient C_{Lmax} to avoid performing in a zone close to stall
- Take-off velocity as the stall one with a safety factor of 20% in accordance with Equation 12 with the purpose of taking off before the 40 m bonus, reducing the C_{Lmax} due to the ground effect

$$V_{to} = 1.2 \sqrt{\frac{2W}{\rho S_w C_{Lmax}}} \quad (12)$$

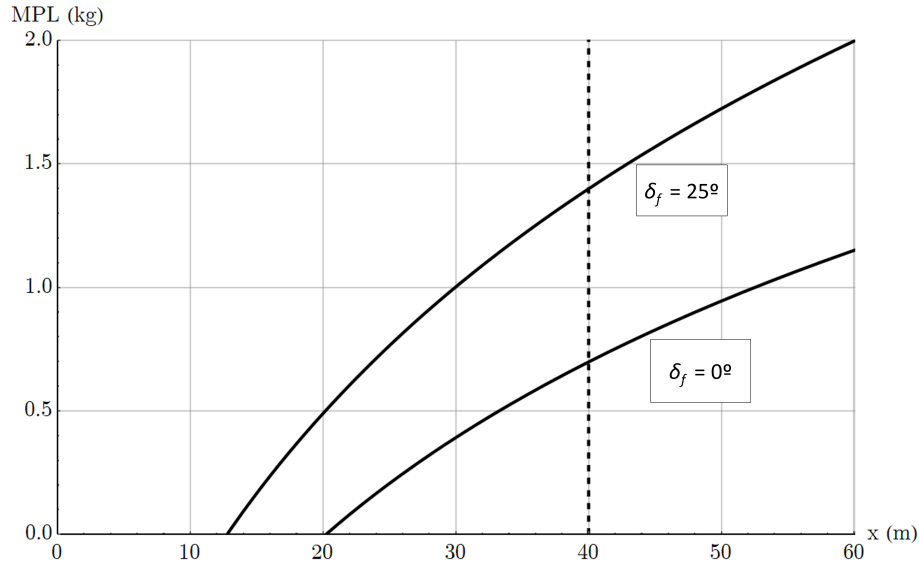


Figure 26: Payload as a function of take-off distance and flap extension

9.3 Climb

The climb stage is modelled through a balance of tangential forces. Assuming a quasi-stationary flight ascent ratio, its expression is given in Equation 13. Considering the stall limit, it is plotted in Figure 27, which verifies that the maximum velocity of ascent with the MTOW is superior to the objective of 2 m/s.

$$V_z \approx \frac{T_s(V) - D(V)}{W} V \quad (13)$$

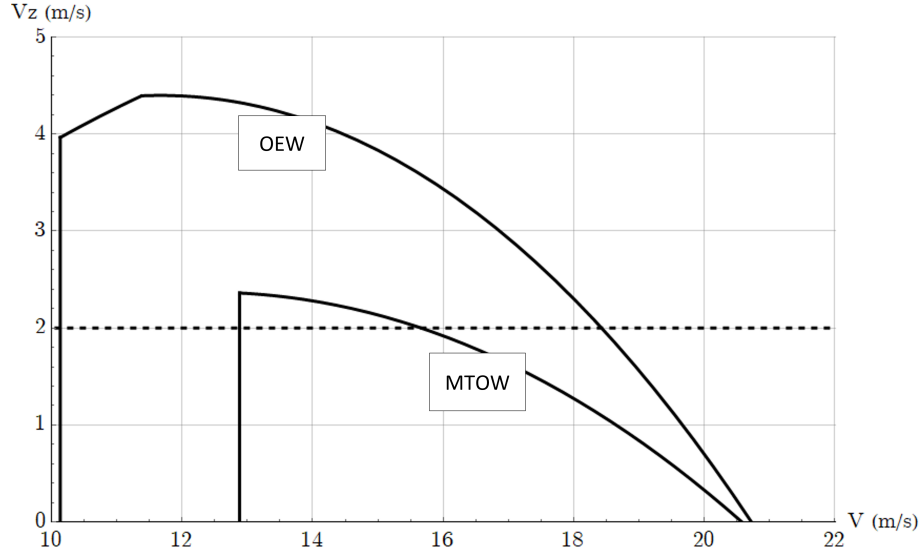


Figure 27: Rate of climb for different payloads

9.4 Cruise Flight

Cruise conditions in Equation 14 are obtained from the balance of tangential and normal forces assuming horizontal and levelled flight at maximum power. Additionally, the total distance d_{cr} if the whole flight was carried out in this conditions is seen in Equation 15.

$$V_{trim} = 20.62 \text{ m/s} \quad C_{Ltrim} = 0.378 \quad (14)$$

$$d_{cr} = V_{cr} \cdot t_{cr} = 2474 \text{ m} \quad (15)$$

The flying area can be flown by means of straight lines of approximately 600 m and turns of 180° with a maximum radius of 65 m in the limit case. The necessary turns to complete it can use the potential energy acquired during the ascent to mitigate the loss of velocity. This is studied with the equilibrium of tangential and normal forces, and additionally, Equation 16 that defines the minimum turning radius R as a function of the roll angle ϕ .

$$R = V \left(\frac{g}{W} \frac{\sin \phi}{V} L \right)^{-1} \quad (16)$$

This expression is plotted in Figure 28 for different roll angles. The maximum values of altitude loss and load factor in this case are seen hereunder.

$$\begin{cases} \phi = 30^\circ \rightarrow \Delta h = -19.20 \text{ m} \\ \phi = 60^\circ \rightarrow n = 2 \end{cases} \quad (17)$$

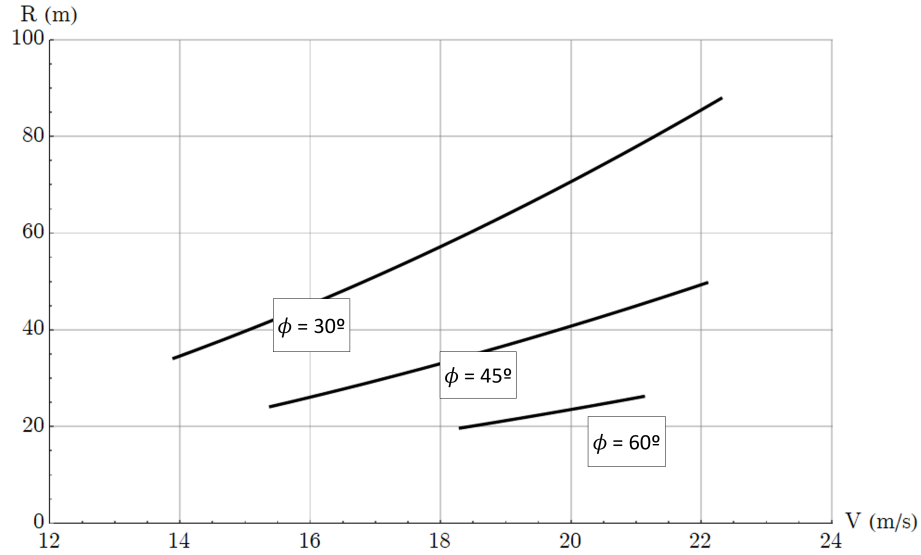


Figure 28: Turning radius for a descent slope of -3° as a function of the roll angle and flight velocity

9.5 Payload Estimation

The lineal function to estimate the maximum payload MPL in kg as a function of ρ in kg/m^3 is given by Equation 18 and is represented in Figure 29.

$$MPL(\rho) = MTOW(\rho) - OEW = \frac{1}{g} \left(\frac{1}{2} \rho S_w V_{to}^2 C_{Lmax} - OEW \right) \rightarrow \quad (18)$$

$$MPL(\rho) = -2.271 + 3.085\rho$$

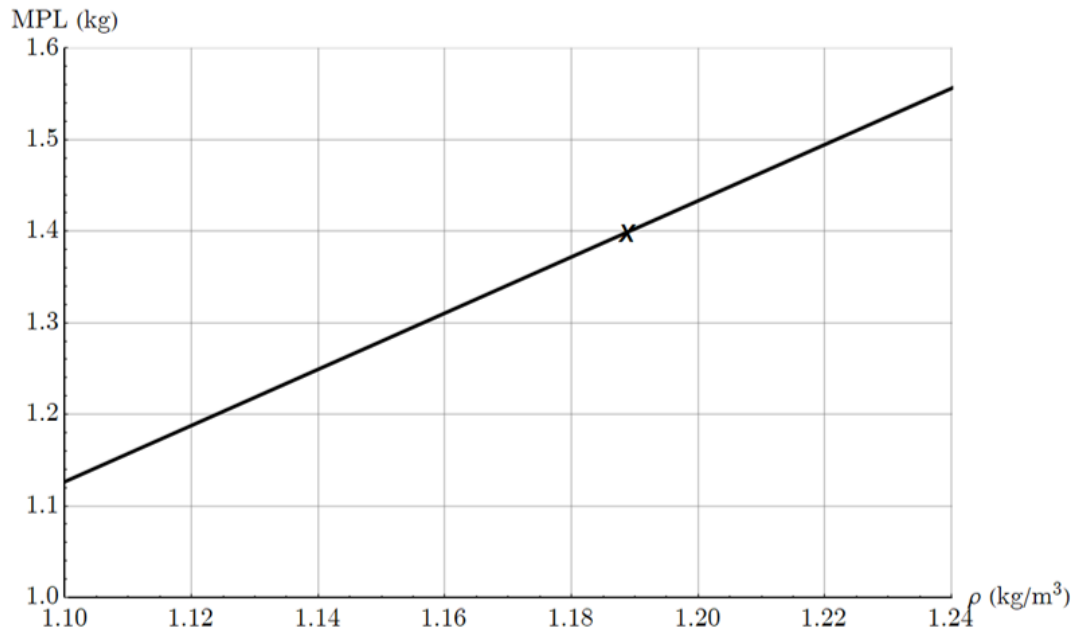


Figure 29: Payload estimation as a function of air density

10 Conclusion and Outlook

The present technical report summarizes the design and manufacturing of the Xtra23 “Favara” prototype by the Xtra2 UPV team to compete in the Air Cargo Challenge 2022. Since the plane has already been manufactured, further tests will be carried out in the upcoming months. The remaining time left until the competition will be dedicated to testing the plane so that the pilot gets used to it while practicing the flight circuit, and also on training important aspects for the competition such as the minimization of loading and unloading times.

For us it is an honour to participate in the ACC 2022, in which we intend to demonstrate all the work and effort that has been put into the project. Our expectations on the competition are optimistic; we aspire to greatly improve our last result on ACC 2019. On the process of preparation for the ACC, we have increased our understanding of aerodynamics, learnt how to work with composites, improved our manufacturing methods and, ultimately, deepen our knowledge in the enthralling world of aeromodelism. We are specially proud of the teamwork and cooperation that have been boosted along with other soft skills, and looking forward to the competition in Munich.

Bibliography

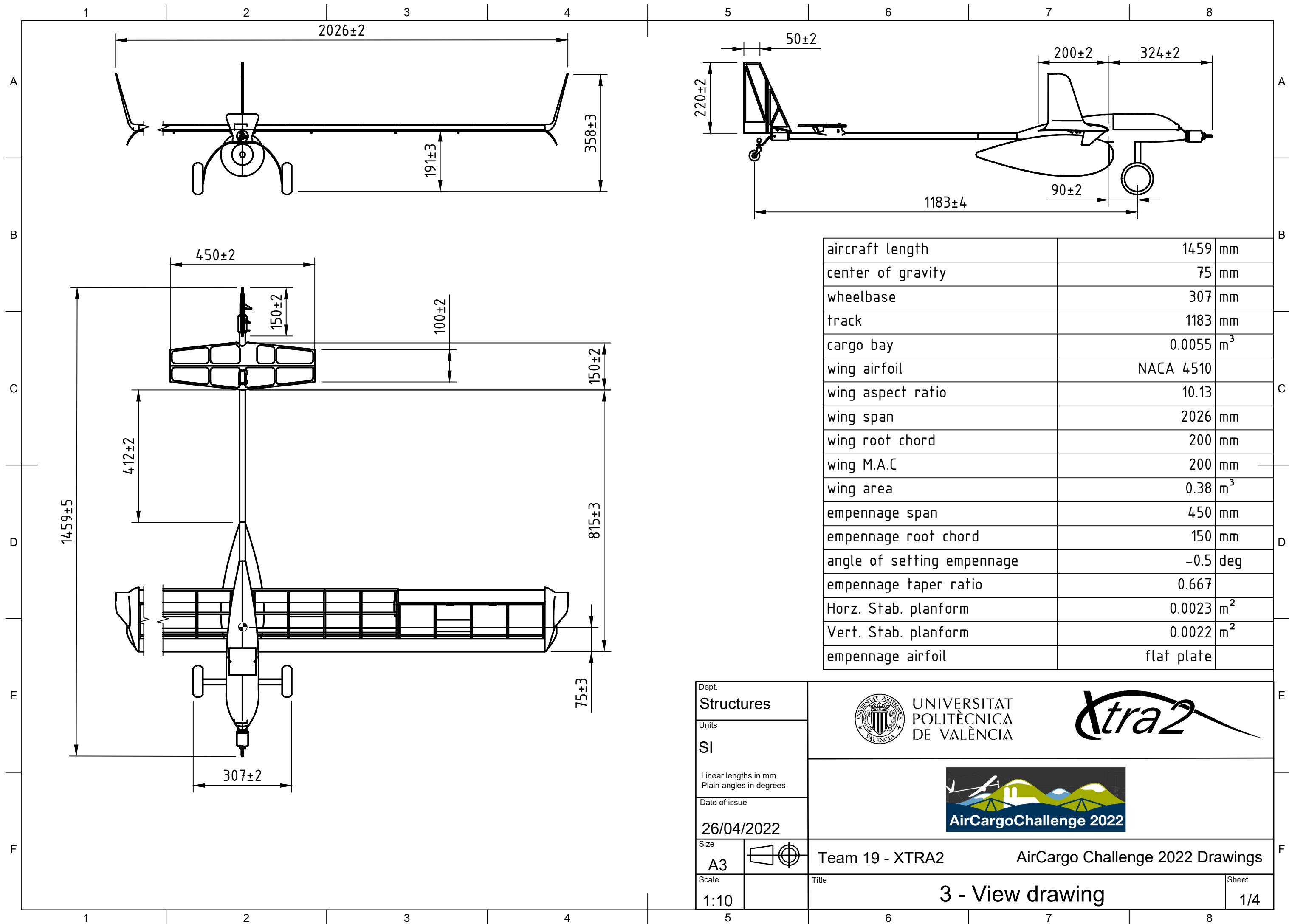
- [1] TEAM AKAMODELL MUNCHEN. *Air Cargo Challenge 2022: Participation Handbook*. 2020. URL: <https://akamodell-muenchen.de/air-cargo-challenge-2022/regulations/>.
- [2] APC-PROPELLERS. *PERFORMANCE DATA*. 2014. URL: <https://www.apcprop.com/technical-information/performance-data/>.
- [3] *Airfoil database search*. 2021. URL: <http://airfoiltools.com/search/index>.
- [4] Mohammad H Sadraey. *Aircraft design: A systems engineering approach*. John Wiley & Sons, 2013.
- [5] C. GLADD. *Servo Torque Calculation*. 2014. URL: <https://www.mnbigbirds.com/Servo%20Torque%20Caculator.htm>.
- [6] A. ALMEIDA GOMES. *Development of an UAV for the Air Cargo Challenge 2017 Competition*. Universidade da Beira Interior, 2017.
- [7] TEAM AKAMODELL MUNCHEN. *ACC 2019*. 2019. URL: <https://akamodell-muenchen.de/en/projekte/alte-projekte/air-cargo-challenges/acc-2019/>.

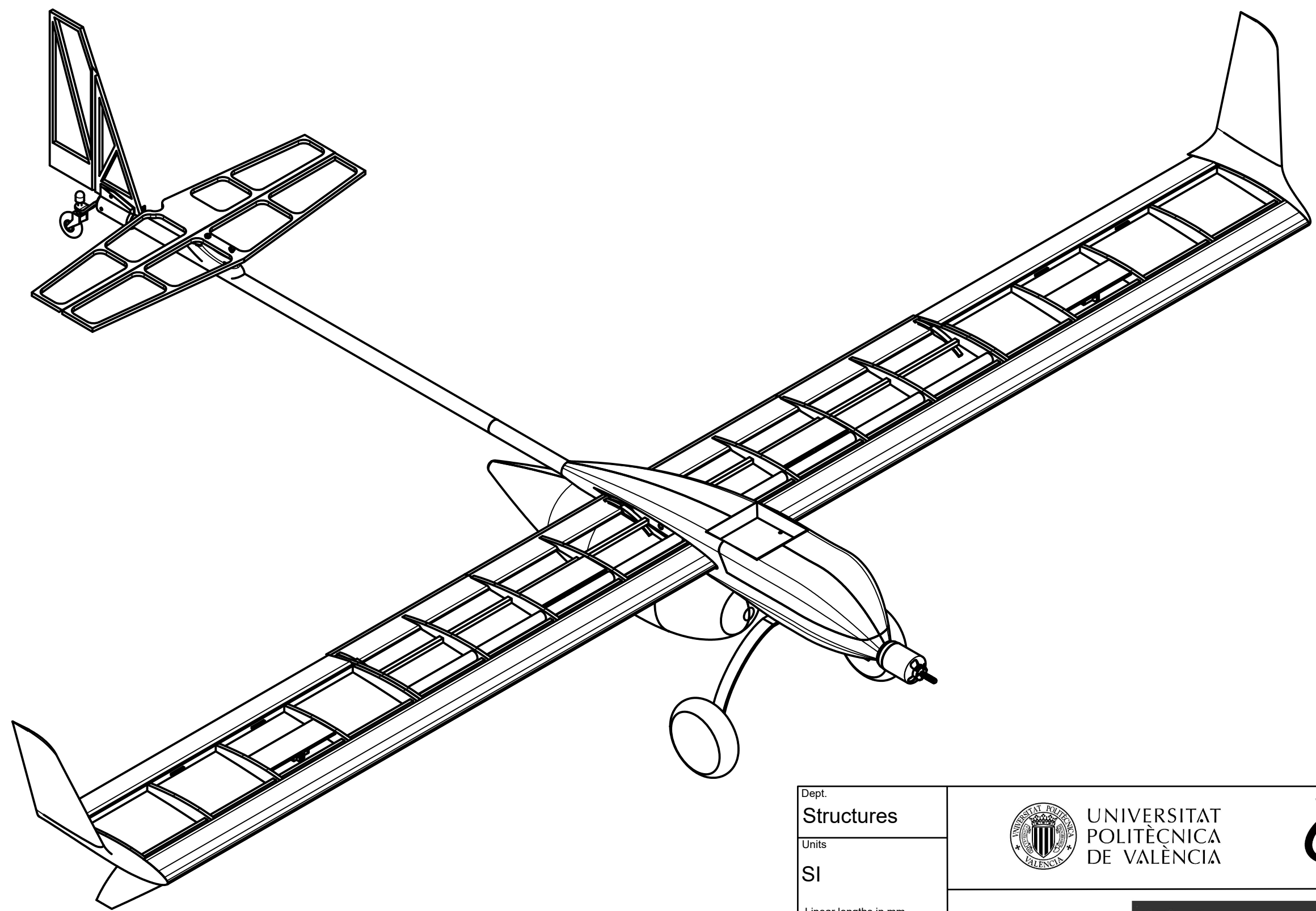
Appendixes




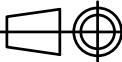
A Similar Aircraft

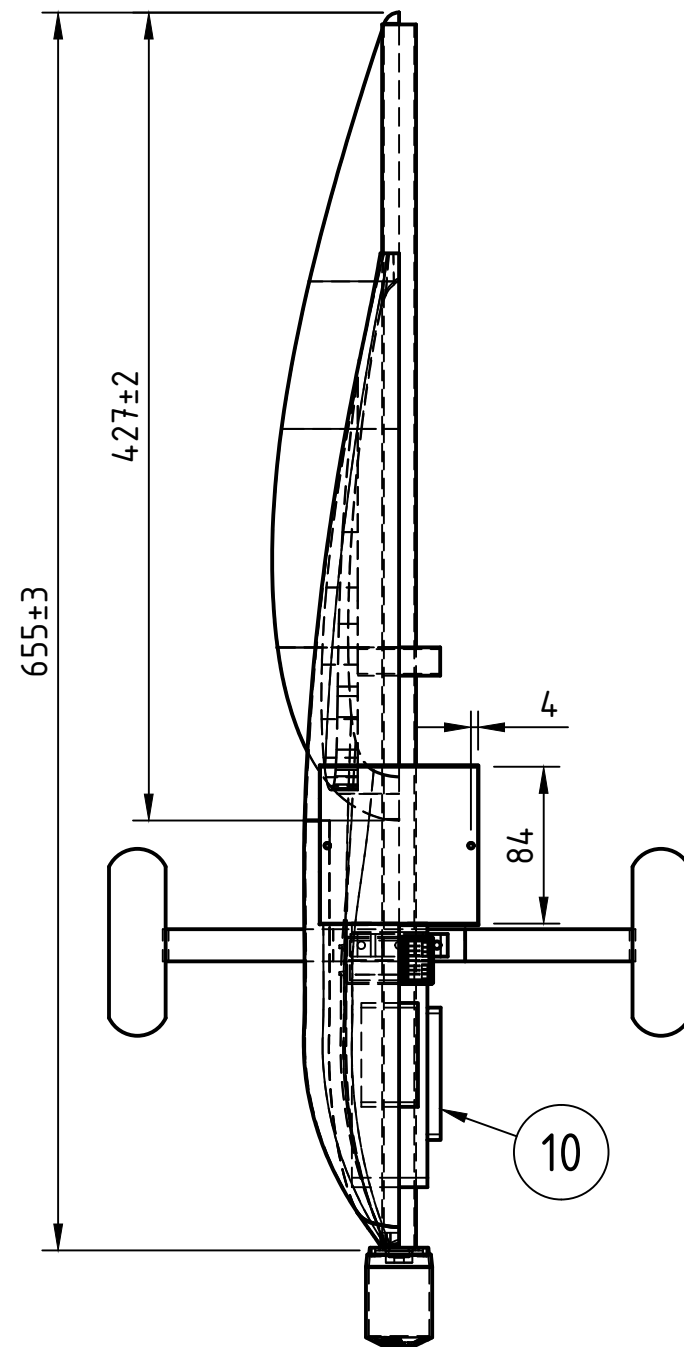
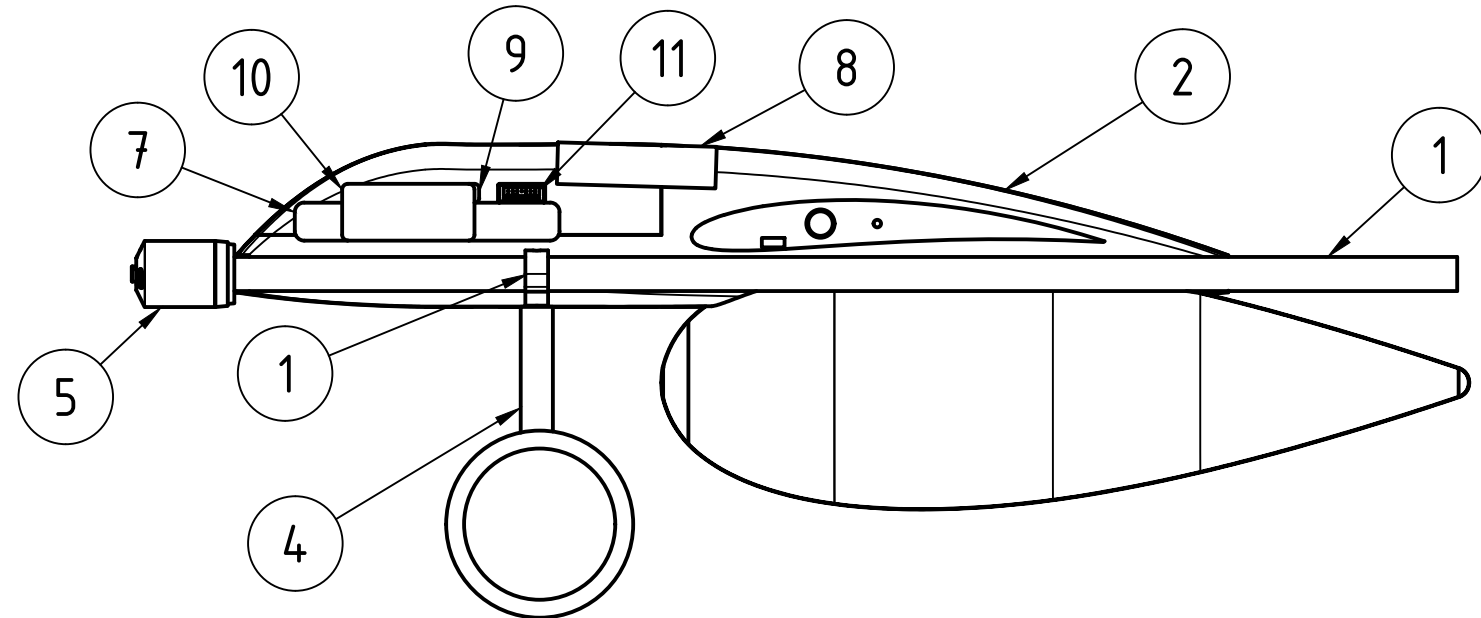
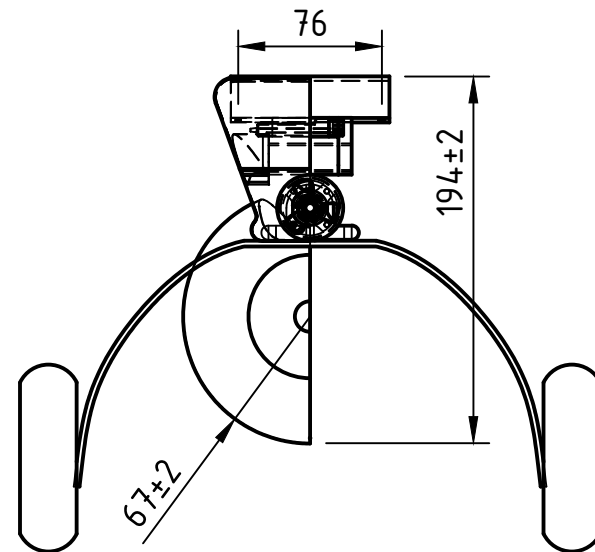
	<i>Garfield</i>	<i>MARS</i>	<i>AKAmodell</i>	<i>Steffi V2</i>	<i>Xtra21</i>
Team	AkaModell Munich	AERO@UBI	AkaModell Stuttgart e.V.	AkaModell Munich	Xtra2 UPV
Year	2019	2017	2017	2015	2020
ACC Result	1 ^o	23 ^o	1 ^o	2 ^o	-
Motor	AXI 2826/10	AXI 2826/10	AXI 2826/10	AXI 2826/10	Cobra 2826/12
Propeller	13 x 7"	13 x 7"	13 x 7"	13 x 7"	12 x 6"
OEW	-	3.39 kg	3.20 kg	-	3.02 kg
m_w	-	2.3 kg	-	-	1.80 kg
MPL	9.80 kg	12.75 kg	10.20 kg	11 kg	-
Wing Structure	CF Shell	CF sandwich, balsa wood and CF	Composite material shell	CF shell biplane	Laminated and CF
S_w	1.28 m ²	1.00 m ²	1.20 m ²	2.00 m ²	1.0 m ²
b_w	4.20 m	4.20 m	3.90 m	2.45 m	2.86 m
c_w	0.31 m	0.25 m	0.31 m	0.40 m	0.35 m
AR_w	13.76	17.62	12.68	6.00	8.18
x_{CG}	44.54 %	31.03 %	-	-	39.71 %
Aerodynamic Profile	ACC_19_v02	MS101_383 MST113_310	-	S1223 modified	NACA CYH
Empennage	V config.	Conventional	T config.	V config.	T config.
V_{stall}	-	32.40 km/h	-	-	40.71 km/h
V_{cr}	62.07 km/h	86.40 km/h	80 km/h	65 km/h	76.17 km/h

B Drawings



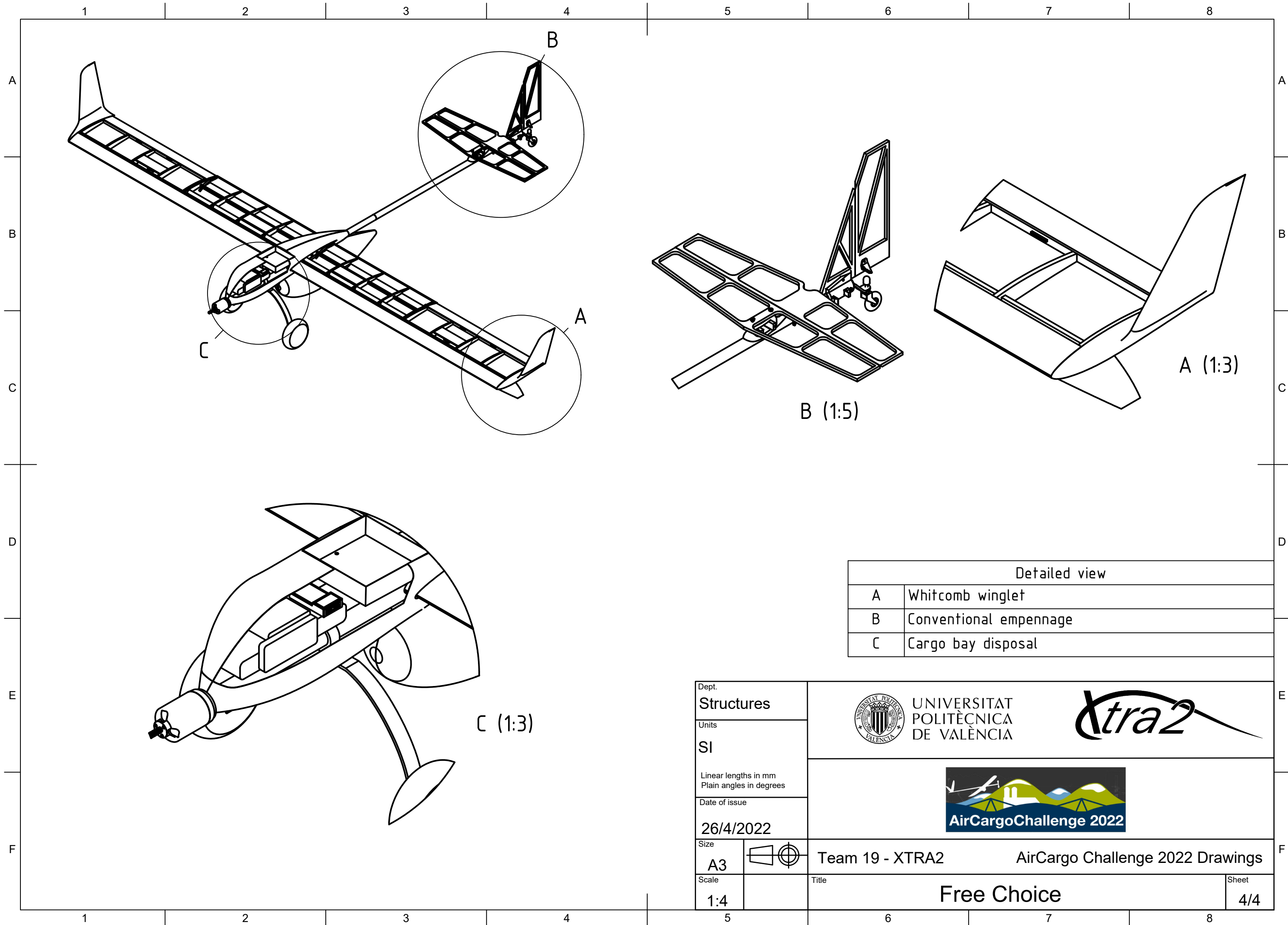


Dept. Structures		 <div>UNIVERSITAT POLITÈCNICA DE VALÈNCIA</div>			
Units SI					
Linear lengths in mm Plain angles in degrees					
Date of issue 26/04/2022					
Size A3		Team 19 - XTRA2		AirCargo Challenge 2022 Drawings	
Scale 1:5		Title Isometric view			Sheet 2/4



LIST OF PARTS			
ID NUMBER	Name	Description	Material
1	Fuselage	Connects all elements together	Carbon Fiber
1	Landing gear support	Absorbs landing gear loads	Aluminum
2	Cargo bay	Fits the payload	Carbon Fiber
4	Landing gear	-	Carbon Fiber
5	Motor	AXI 2826/ 10 GOLD LINE V2	-
7	Main battery	Powers the motor	-
8	Measuring equipment	Fits the competition gps	Carbon Fiber
9	ESC	Controls power input to the motor	-
10	Secondary battery	Power the electronics	-
11	RC Receiver	Receives signal from control station	-

Dept. Structures		 UNIVERSITAT POLITÈCNICA DE VALÈNCIA 	
Units SI			
Linear lengths in mm Plain angles in degrees			
Date of issue 26/4/2022			
Size A3		Team 19 - XTRA2	AirCargo Challenge 2022 Drawings
Scale 1:5		Cargo Bay	Sheet 3/4



Detailed view	
A	Whitcomb winglet
B	Conventional empennage
C	Cargo bay disposal

Dept. Structures		 UNIVERSITAT POLITÀCNICA DE VALÈNCIA			
Units SI					
Linear lengths in mm Plain angles in degrees					
Date of issue 26/4/2022					
Size A3					
Scale 1:4		Team 19 - XTRA2		AirCargo Challenge 2022 Drawings	
		Title Free Choice			Sheet 4/4